NTNU – Trondheim
Norwegian University of
Science and Technology

CFD study of a rotating gas-liquid separator

Design og bygging av flere mikro-dråpe generatorer

Mari Stene

Master of Science in Mechanical Engineering
Submission date: June 2013
Supervisor: Carlos Alberto Dorao, EPT

Norwegian University of Science and Technology
Department of Energy and Process Engineering

NTNU
Norwegian University
of Science and Technology

Department of Energy
and Process Engineering

EPT-M-2013-111

MASTER THESIS

for

Stud.techn Mari Stene
Spring 2013

CFD study of a rotating gas-liquid separator

Design og bygging av flere mikro-dråpegeneratoren

Background and objective

Removing liquids from a gas stream is very important in gas processing applications, especially in the oil and gas industry. Effective removal of these contaminants can prevent costly problems and downtime with downstream equipment like compressors, turbines and burners.

CFD tools can provide a valuable support for the design and evaluation of the performance of the separators. However due to the complex phenomena involved in the separation process, the reliability of the CFD models is rather limited. A particular issue is the capability of the CFD tools for predicting the behavior of the droplets and its interactions with the demister and the surfaces inside the separator.

In this work the main goal is to set a CFD model of a rotating gas-liquid separator and identify the main drawback of the available models

The following tasks are to be considered:

1 Literature review of droplet dynamics related to separators, with focus on
   a) Dynamic of the droplets in different regions of the separators (dominant effects)
   b) Available correlations for describing the dominant process
2 Set the CFD model, and perform simulations of the model.
3 Perform error analysis an discuss the validation of the model

-- " --

Within 14 days of receiving the written text on the master thesis, the candidate shall submit a research plan for his project to the department.

When the thesis is evaluated, emphasis is put on processing of the results, and that they are presented in tabular and/or graphic form in a clear manner, and that they are analyzed carefully.

The thesis should be formulated as a research report with summary both in English and Norwegian, conclusion, literature references, table of contents etc. During the preparation of the text, the candidate should make an effort to produce a well-structured and easily readable report. In order to ease the evaluation of the thesis, it is important that the cross-references are correct. In the making of the report, strong emphasis should be placed on both a thorough discussion of the results and an orderly presentation.

The candidate is requested to initiate and keep close contact with his/her academic supervisor(s) throughout the working period. The candidate must follow the rules and regulations of NTNU as well as passive directions given by the Department of Energy and Process Engineering.

Risk assessment of the candidate's work shall be carried out according to the department's procedures. The risk assessment must be documented and included as part of the final report. Events related to the candidate's work adversely affecting the health, safety or security, must be documented and included as part of the final report. If the documentation on risk assessment represents a large number of pages, the full version is to be submitted electronically to the supervisor and an excerpt is included in the report.

Pursuant to "Regulations concerning the supplementary provisions to the technology study program/Master of Science" at NTNU §20, the Department reserves the permission to utilize all the results and data for teaching and research purposes as well as in future publications.

The final report is to be submitted digitally in DAIM. An executive summary of the thesis including title, student's name, supervisor's name, year, department name, and NTNU's logo and name, shall be submitted to the department as a separate pdf file. Based on an agreement with the supervisor, the final report and other material and documents may be given to the supervisor in digital format.

X Work to be done in lab (Water power lab, Fluids engineering lab, Thermal engineering lab)
☐ Field work

Department of Energy and Process Engineering, 16. January 2013

Olav Bolland
Department Head

Carlos A. Dorao
Academic Supervisor

Research Advisors: Nicolas La forgia

Preface

This thesis is a result of a master project at Department of Energy and Process Engineering at Norwegian University of Science and Technology (NTNU). The work is carried out over 20 weeks during spring semester 2013.

Trondheim, 10. Juni 2013

Acknowledgements

I would like to thank Professor Carlos Alberto Dorao for his guidance, help and support throughout the project, and for the introduction to and tutorials in ANSYS FLUENT.

Abstract

Extracting Natural Gas from the reservoirs and transporting it to shore requires the gas to be pure from liquids and contaminants. These contaminants can be extracted from the gas by separators. A new separation technology, the Lynx separator, has been developed at NTNU, where a rotating element inside the separator is to capture liquid particles and introduce a centrifugal force for increasing the separation efficiency. The knowledge on how this element influences the flow and performs is limited, and there are no known experiments performed on this system per today. Using CFD tools to construct a suitable model can contribute to increase the knowledge on how this capturing element impacts the flow.

The work presented in this thesis has been looking into the structure of metal foams used as the separation mechanism in Lynx separator. A model of a single tetrakaidecahedron cell representing a microstructure of the real life foam geometry has been constructed in ANSYS Mechanical APDL and further included in ANSYS FLUENT, where three cells were united as one element with a capturing cylinder around to represent a simple small scale model of the separator.

By turbulent k-ω modelling in combination with the Discrete Phase Model, simulations on gas-liquid flow represented by air with inert water particles of different diameters has been calculated upon, where the focus has been set on the interaction between the particles and the metal foam cells. Different cases have been investigated where the capturing element has been set into different angular velocities to quantify the impact on the gas flow and particle behaviour.

The presented model shows the influence of the different rotating velocities on both gas and particle flow. The capture of particles with a stationary metal foam is mainly limited to larger particles with a diameter of 100 μm and 500 μm. Introducing a centrifugal force results in swirling flow for both gas and larger particles, reducing the interaction of larger particles with the metal foam cells as these swirl out towards the walls. The flow of 10 μm particles has a radial displacement as a result of colliding with the metal foam, separating them from the gas, while capture of 1 μm has showed to be very limited. Introducing a very high rotational velocity has shown to reduce the reliability of the proposed model, and it cannot be verified that this model is reliable as the rotational velocity exceeds 2000 rotations per minute.

Sammendrag

Utvinning av naturgass finner ofte sted offshore og gassen må transporteres lange distanser for å nå land. Et kriterie for å kunne transportere denne gassen er at den er ren fra olje, vann og andre forurensninger. Disse forurensningene kan utvinnes fra gassen ved gass-væske separatorer.

Som et resultat av dagens høyteknologi og økt kunnskap utvikles det stadig nye komponenter hvor det er ønskelig å redusere størrelsen på separatorene, samt gjøre det mulig med høyere massestrøm uten at dette reduserer utskillingen. En ny teknologi, Lynx separator, er utviklet ved NTNU hvor et roterende utskillingselement er plassert inne i separatoren for å fange opp uønskede partikler. Som et resultat av rotasjonen dannes det også en sentrifugal kraft som bidrar til utskilling av partiklene. Det er per dags dato ikke utført noen eksperimenter på dette systemet, og kunnskapen om hvordan dette roterende elementet påvirker gass-væske flyten og fanger opp de ulike partikkel størrelsene er meget begrenset. Ved å konstruere en representativ modell og utføre simuleringer ved hjelp av CFD programmer, kan dette bidra til å øke forståelsen av hvordan gassen og partiklene påvirkes av de ulike komponentene og kreftene som virker i systemet.

I denne hovedoppgaven har fokuset vært satt på strukturen av utskillingselementet, også kalt fibernett, hvor hovedmålet har vært å se på hvordan dette fibernettet påvirker partiklenes bevegelse gjennom separatoren. Fibernett har en kompakt struktur og består vanligvis av tusenvis av små celler. En modell av én celle er konstruert i ANSYS Mechanical APDL som et tetrakaidecahedron og videre brukt i ANSYS FLUENT, hvor tre celler er satt sammen som en enhet omringet av en sylinder for å representere en mikroskopisk modell av separatoren.

Ved bruk av turbulent k-ω modell og diskret fase modell (DPM) i FLUENT er det utført simuleringer av gass-væske strømninger representert av luft med vann partikler av ulik diameter. Fibernettet er satt i varierende rotasjonshastighet for å undersøke hvilken påvirkning dette har på gass strømmen og partikkel bevegelsen.

Den forslåtte modellen viser at partikler med mindre diameter enn 10μm ikke lar seg skilles ut fra gassen hverken ved et stasjonært element eller ved innføring av en sentrifugalkraft. Det stasjonære fibernettet skiller ut partikler ved 100μm og 500μm. Ved en innføring av rotasjon på 2000 rpm, kan partikler på 10μm også skilles ut. Partikler med en diameter på 1 micron har vist seg å være vanskelig å skille ut ettersom de ikke påvirkes av det roterende elementet, men følger gass

strømmen. Ved ekstrem høy roterende hastighet, har påliteligheten til den foreslåtte modellen vist seg å reduseres, og det kan ikke kvantifiseres at denne modellen egner seg for roterende hastigheter større enn 2000 rotasjoner per minutt.

Contents

List of Figures

List of Tables

Nomenclature

Δ	Difference
η_{st}	Single target efficiency [%]
μ	Micron [10^{-6}]
μ_g	Gas viscosity [N/ms]
ω	Angular velocity [rpm]
ρ_g	Density gas [kg/m^3]
ρ_l	Density liquid [kg/m^3]
ρ_{RD}	Relative density metal foam
σ	Surface tension [N/m]
τ	Residence time [s]
ε	Turbulent dissipation
ξ	Efficiency
a_c	Centripetal acceleration [m/s^2]
A_d	Particle surface area [m^2]
d_p	Droplet/particle diameter [m]
F_d	Drag force [N]
F_g	Gravitational force [N]
g	Gravity [m/s^2]

k	Kinetic energy $[N]$
L	Length $[m]$
N_{layers}	Number of layers
P	Pressure $[Pa]$
PPI	Pores per inch
Q	Volumetric flow rate $[kg/s]$
r	Circular radius $[m]$
r_l	Distance from radius to radial inlet position of particle $[m]$
r_p	Droplet/particle radius $[m]$
r_{wall}	Distance from radius to wall $[m]$
Re	Reynolds number
rpm	Rotations per minute
S_{mesh}	Mesh specific surface area $[m^2]$
T	Temperature $[K]$
u_θ	Tangential velocity $[m/s]$
u_g	Gas velocity $[m/s]$
u_r	Radial settling velocity $[m/s]$
$U_{terminal}$	Terminal velocity $[m/s]$
V	Liquid velocity $[m/s]$
v	Relative gas liquid velocity $[m/s]$
V_g	Superficial gas velocity $[m/s]$
V_p	Droplet/particle volume $[m^3]$
We	Weber number
h	Metal foam height $[m]$
U	Particle velocity $[m/s]$

Chapter 1

Introduction

1.1 Motivation

The petroleum sector has great impact on the Norwegian industry and economy. Within this sector, the export of oil and natural gas is one of the main elements. When natural gas is extracted from the reservoirs, it contains contaminants like oil, hydrocarbons, water, CO_2 and H_2S. As this is transported through the pipelines, these contaminants may cause damages like hydrate and wax formation. In order to reduce these damages and make the transportation possible, the gas must be pre-treated. This pre-treatment can be done by use of gas scrubbers that separates the gas and the liquid. Together with heat exchangers and compressors, the treatment with scrubbers is the most important process for obtaining the hydrocarbon dew point specifications in an offshore plant. The main purpose of these gas scrubbers is to remove smaller amount of liquid from the gas. If the amount of liquid is above 5 volume%, the vessel is no longer referred to as a gas scrubber, but a separator [5].

In recent times, more complex separators have been introduced, utilizing higher technologies, where different types are the cyclonic separator and the rotating particle separator. These have been introduced as an alternative to traditional separators, being able to handle higher velocities of the incoming flow, separating smaller particles, handling larger amount of liquid entrained within the gas and reducing the size of the vessels.

1.1.1 Rotating particle separator

The principle of the rotating particle separator is a cylinder with a filter element packed with several axial channels rotating around a common axis. As the particles are entering the element, they are centrifuged out towards the walls of the surrounding cylinder [6]. This separator was originally meant for separating particles from gas, only it has been marketed and used for liquid-liquid separation, and not within the gas market.

1.1.2 Lynx Separator

Lynx Separator is a new technology developed by Dorao and Fernandino at NTNU. The Lynx separator is a vertical separator that works like a conventional, only with a rotating mesh pad. A capturing storage box surrounds the rotating element. Unlike the conventional separators where the gravitational force is the main separation force, this separator also introduces the effect of centrifugal force, with an important impact on the droplet separation. The two main mechanisms of separation in this vessel is then the cyclonic separation by centrifugal force and droplet capture by the rotating aluminum mesh pad. The goal of this separator is to be able to reduce the size of the vessel and hopefully the cost, without this reducing the efficiency. The rotating mesh pad creates a centrifugal field where the liquid droplets are forced into the surrounding wall, allowing the liquid to enter the separator in a higher speed and larger amount than for a conventional separator. The mesh pad will be referred to as metal foam from here.

This is a newly developed technology where no experiments or simulations have previously been performed, and the knowledge on how this system performs and the rotating element influences the gas-liquid flow is highly limited.

1.2 Thesis objectives

The aim of this thesis is to increase the knowledge of gas flow and liquid particle behaviour in interaction with solid cavity within the Lynx separator. Focus is set on the influence of the rotating element on the particles and the gas, and the impact this obstacle has on the flow, where the goal is to separate the particles from the gas.

1.3 Scope

The work performed in this thesis includes a study looking into the structure of metal foams in order to create a small scale model based on one single cell in a metal foam. Three cells has further on been united as one element to create a metal foam layer. A cylinder surrounding this element completes the structure representing the Lynx separator.

Simulations in ANSYS FLUENT has been performed for air flowing as a continuum media with inert, spherical water particles with a diameter range of 1μm to 500μm. The cells representing the metal foam is set into different rotational velocities of 0, 200, 2000 and 10000 rpm. To compute these simulations, turbulent k-ω model is utilized in combination with Discrete Phase Model. Stochastic collision, coalescence and particle breakup are enabled to make the simulation as realistic as possible.

In order to perform these simulations, a fine mesh has been created in ANSYS Meshing. Consisting of tetrahedrons with 852221 nodes and 617371 elements. The validation of mesh quality has been based on cell skewness and orthogonal quality.

1.3.1 Thesis Outline

Chapter 2 gives an introduction to the porous media working as the separation element within the separator, and its geometrical structure.

In Chapter 3 a review of background, literature and fundamentals of droplet motion, forces and equations regarding particles and the flow of particles entrained in gas are presented.

Chapter 4 presents the fundamentals behind CFD calculations and the available and suitable models for this case.

Chapter 5 presents the proposed model for simulations as well as simulation results, discussion and validation. A conclusion and suggestions for further work is given in Chapter 6

Chapter 2

Metal foam

2.1 Definition of metallic foam

The use of metal foams are steadily increasing due to it‘s advantageous characteristics and properties. Industrial areas such as heat exchangers, separators and aerospace, among others, have for a long time exploited the low density, light weight, high strength and high thermal conductivity of metal foams. In addition to these characteristics, the porosity and permeability makes the foam an efficient component. While there as so many good qualities and advantages of using metal foams, the use of it also requires good insight in both geometry and fluid flow behaviour in order to achieve good results within the area of usage.

2.2 Metal foam geometry

Metal foams can be classified as either open cell or closed cell foams. The open cell foam has cell walls with open holes, also called pores in between, allowing fluid freely to pass through. The closed cell on the other hand, has closed walls without any open holes or pores.

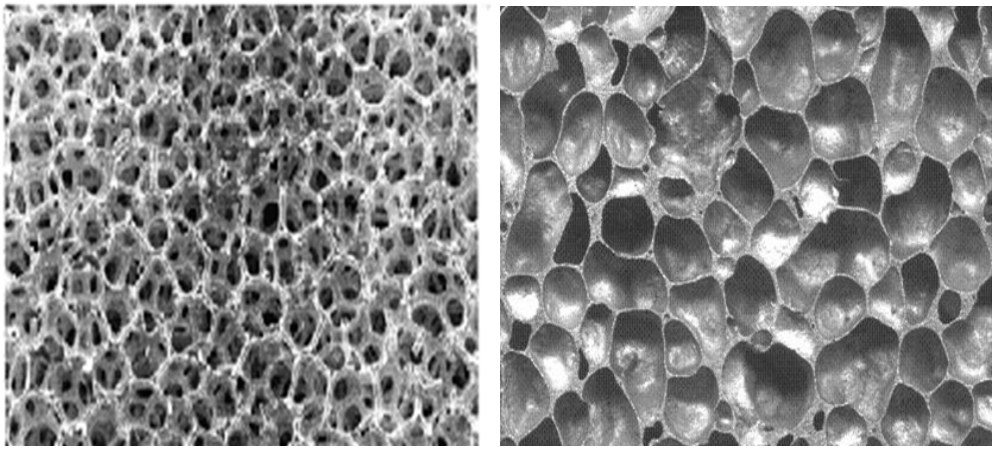

Figure 2.1: Open cell metal foam and closed cell metal foam. (www.ultramet.com, 2013)

Within the Lynx separator, an open cell metal foam is utilized. Based on this, the focus will be set on the geometry and structure of open cell metal foams exclusively. The geometry and characteristics of open cell metal foams is dependant on the producer and production process, but even with different manufacturers, foams usually hold some similarities. The overall geometry are often presented quite similar, as the majority of foams used in this period of time are constructed as a composition of multiple tetrakaidecahedrons [3]. However, the geometry of real open cell foams often differ from the idealistic geometry, and many researchers have looked into different foam structures aiming towards developing a uniform model describing the physical geometry and characteristics.

This has been investigated in several studies, where one of the most popular areas of usage for the metal foam is within heat transfer modelling, due to the foams good thermal qualities. Studies have been made looking further into the structure of real metal foams.

In order to look closely into the structure, a x-ray microscopic tomographic image method is often found to be used, in such a way that an image is taken of a real life metal foam and software programs are utilized for analysing structures from these images. Thiyagasundaram et al [12] found through their microscopic image that the structure could in fact be approximated as a tetrakaidecahedron and this

would represent the metal foam quite well.

Such software and x-ray tomographic equipment has not been available in this study, and the structure of one single cell is set to match a tetrakaidecahedron.

This structure was presented as early as 1887 by Lord Kelvin, and is sometimes also referred to as the Lord Kelvin structure. The tetrakaidecahedron was mainly decided upon based on experimental work and not mathematically proven to be the most optimal structure.

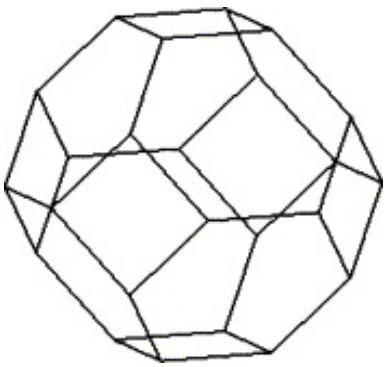

Figure 2.2: Tetrakaidecahedron (ScienceDirect, 2013)

2.2.1 ERG Duocel Metal Foam

The foam used in the Lynx separator is the ERG Duocel Metal Foam, distributed by ERG Materials and Aerospace Corporation. This is an open cell aluminum metal foam alloy 6101-T6 which is manufactured to be homogeneous and isotropic and is quite often used in the industry today.

The properties of these foams are strongly related to the relative density. Relative density is the mass of real material in a block of foam compared to what it would be if it were a solid block of the same material [3]. As the relative density increases, the diameter of the ligaments increase and the foam structure becomes stronger. Typical relative densities for Duocel metal foams are in the range of 3% to 10%.

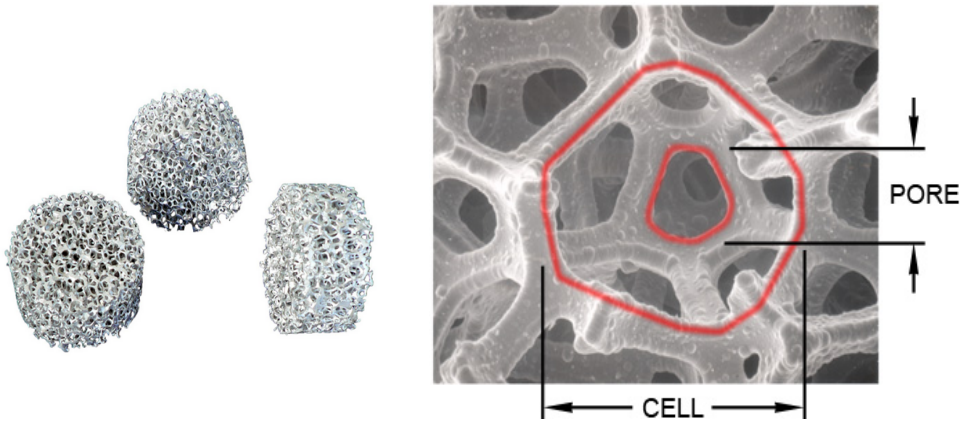

Figure 2.3: Metal foam structure (ERG Aerospace, 2013)

Each cell consists of 14 facets where the opening through each of these are called pores. The number of pores per inch of the foam is referred to as the pore size, which is one of the most important characteristics of the foam, and defined the number of cells for a given length. The vapour passes through the pores, and as it flows through, frictional losses leads to pressure drop. The amount of solids inside the foam is important, the greater amount, the larger the surface where liquid flows, which again gives larger pressure drop as a result of friction. Available volume of flow is called porosity or voidage. The droplets flowing through the metal foam is forced to change direction several times, and forces acting between the metal wires and particles influence the outcome.

In general, ERG Duocel metal foams are manufactured with 5 to 40 pores per linear inch (PPI). The pore size defines how fine or coarse the foam is. The lesser number of PPI, the more open and coarse the foam will appear. Usually the diameter of the pores are set to be 50-70% of the larger cells diameter [3].

Chapter 3

Principles of droplet motion

In this chapter, the forces acting on droplets/particles will be discussed. General expressions for particles moving within gas is presented, as well as the influence of centrifugal force and external force on the particles.

3.1 Basic particle forces

By the laws of fluid mechanics, the motion of a particle within a gas, can be predicted. The particle is carried by the flow of the surrounding gas, following the gas trajectories, this due to the drag force acting from the gas on the particle.

If the particles are to separate from the gas flow, external forces are needed. These forces must exceed the drag force. Within traditional vertical gas-liquid separators, this external force is the gravitational force. As a result of this, the particles are under the influence of two opposing forces, drag force acting in the same direction as the gas flow, and the gravitational force acting in the opposite direction.

$$mass \times acceleration = m\frac{du}{dt} = F_{body} + F_{drag} + F_{unsteadyforceterms} \tag{3.1}$$

Body force is usually gravitational force and/or centrifugal force. Fluid drag is the drag force acting on the particle if it moves with a steady velocity relative

to the fluid. The unsteady terms accounts for acceleration of the particle as the particle moves relative to the fluid.

$$F_{gravity} = F_g = V_p g(\rho_l - \rho_g) \tag{3.2}$$

$$F_{drag} = F_d = 3\pi U d_p \mu_g = 6\pi U r_p \mu_g \tag{3.3}$$

where V_p is the volume of the particle, $\frac{4}{3}\pi r_p^3$, ρ the different densities of the gas and liquid, μ_g is the gas viscosity, U the particle velocity and d_p and r_p the particle diameter and radius. Here, the drag force is based upon Stokes law, considering that the particle is spherical with a small diameter, up to 100 microns. Balancing these two forces working on the spherical particle, the particle is held at stationary position.

$$V_p g(\rho_l - \rho_g) = 6\pi \mu_g r_p U \tag{3.4}$$

Solving equation (3.4) for U, the terminal velocity of the particle can be found. This is the stable velocity the particle reaches after a period of acceleration in a gas flow.

$$U_{terminal} = \frac{2(\rho_g - \rho_l) r_p^2}{9\mu_g} g = \frac{(\rho_g - \rho_l) d_p^2}{18\mu_g} g \tag{3.5}$$

It can be seen from the equation that the terminal velocity is dependant on the diameter of the particle, where smaller particles will reach their terminal velocity after a shorter amount of time than those of a larger diameter. This equation does only hold when the degree of turbulence within the fluid is small, Re<1. And is limited to a upper diameter of 100 microns. Turbulence is based on Reynolds number

$$Re = \frac{D_p U \rho_g}{\mu_g} \tag{3.6}$$

, where the particle Reynolds number gives an indication on the ratio of inertial to viscous forces within the gas, and hence it is the gas properties ρ_g and μ_g that is to be used [8].

3.2 Droplet motion in rotating frame of reference

As the gas liquid mixture flows within a centrifugal field, the particles and surrounding gas are no longer influenced by the same forces, and the gas and liquid does not necessarily follow the same flow trajectories. The centrifugal forces present due to the centrifugal field introduces a radial movement for the particles. When particles are separated from the continuum medium by centrifugal forces, we are referring to inertial separation. In addition, a buoyant force is presence due to the displacement of the particle, this is however insignificant for particles greater than 0.1 microns.

The effect of centrifugal force has been looked into by several studies, where Richard Holdich is one, having presented the forces acting on particles and the movement of these through a centrifugal field [8]. Based on the expression presented in (3.5), in a centrifugal field, the centripetal acceleration a_c introduces a tangential velocity u_t, replacing the effect of gravity. This neglection in gravitational impact can be done by assuming the centripetal acceleration to have such a larger impact than the gravitational force [4] that the gravity can be replaced. As the focus is set on rotation, centrifugal forces and radial movement, cylindrical coordinates will be used, (r,θ,z) instead of Cartesian coordinates in the following expressions.

As the gravitational force no longer is assumed to impact the particle, but the centripetal acceleration to have great influence, the equation (3.5) can be modified into considering centripetal acceleration based on $a_c = \frac{u_\theta^2}{r}$ [8]

$$u_r = \frac{dr}{dt} = \frac{(\rho_l - \rho_g) d_p^2 u_\theta^2}{18 \mu_g r} \tag{3.7}$$

where ρ_l and ρ_g is the density of the liquid and gas respectively, d_p^2 the particle diameter, u_θ the tangential velocity, μ the viscosity of the gas and r the radial position. This equation is based on the assumption that the liquid particles and the surrounding gas are following the same tangential velocity, and the gas velocity to be uniform.

Rewriting (3.7) to take into consideration the axial velocity of the spinning metal foam, assuming the gas to follow the angular velocity of the rotating element, u_θ

can be rewritten into $(r\omega)$, resulting in

$$u_r = \frac{dr}{dt} = \frac{(\rho_l - \rho_g)d_p^2\omega^2}{18\mu_g r} \tag{3.8}$$

Based on this, an expression for the time it takes one particle to reach the wall depending on the radial placement at the inlet can be found [11].

$$t_{radial} = \frac{18\mu_g}{d_p^2(\rho_l - \rho_g)\omega^2} ln(\frac{r_{wall}}{r_l}) \tag{3.9}$$

with r_l being the distance of particle radial inlet position to the centre of the cylinder, r_{wall} the radius of the cylinder and ω the rotational velocity.

From this , one can see that for a given diameter, the time it takes one particle to move a distance equal to the radius of the cylinder decreases as the inlet position relative to the distance from the centre increases. The time also reduces as the diameter of the particle increases.

This equation predicts the flow in a rotational frame of reference. However, it does not take into account the interference of the particles with the wires of the metal foam, which is assumed to influence the trajectories of the particles, making it less smooth.

3.3 Flow around obstacles

In addition to the centrifugal force present due to the rotating element, the wires or fibres constituting the metal foam is assumed to collect the particles, capture them and separate them from the gas flow. The gas however, is assumed to flow around the obstacle and to be ejected at the outlet.

Whether a particle is collected in the metal foam and captured at the surrounding wall or if it flows through or past the metal foam, and exits at the outlet, depends on the particle diameter, velocity of the flow and the radial movement of the particle.

The capturing of particles can be presented in many ways. One way is to look into the single target efficiency,

$$\eta_s t = \frac{r_{critical}}{r} \tag{3.10}$$

where the particle is captured by the single target, which can be fibres or wires within metal foams, by inertial separation. Meaning the gas can change its direction, moving around the obstacle, while the particle has a greater inertia and will move towards the capturing target, collide and separation will take place.

The smallest particles captured will be the once which during the time of flow moves over a radial distance corresponding to the length of the element. An analysis of this was presented by Holdich [8]. The particle being separated by a probability of 50% is the particle entering at R_{50} and reaches the wall at the exit, hence has a radial displacement of $R_{wall} - R_{50}$ over the total cylinder length. Assuming uniform flow and uniform distribution of particles at the inlet, 50% of the particles will enter at a radial position $R_{50} < R_{wall}$ and 50% will enter at a position $R_{50} > R_{wall}$.

The diameter of this particle can be found by equation (3.8) at $r(t) = R_{wall}$ and $r(0) = R_{50}$. Solving for d_p gives

$$d_p^2 = \frac{18\mu_g g(R_{wall}^2 - R_{50}^2)}{2(\rho_l - \rho_g)\int_0^t u_t^2 dt} \tag{3.11}$$

By assuming this, the diameter of the smallest particle being separated can be found.

This equation is based upon a separating element consisting of a number of cylinders where as the particle enters the cylinders, it will experience a radial displacement, and forced out towards the walls. This does not however represent the complex geometry of the open cell metal foam, and this expression does not necessarily match the situation investigated in this case.

3.3.1 Droplet collision dynamics

Particles colliding with a surface, or under a relative influence of two fluids or phases, can be presented by the dimensionless quality, Weber number. For a spherical particle, the Weber number is defined as

$$We = \frac{\rho_g v^2 D_p}{\sigma} \tag{3.12}$$

where ρ_g is the density of the continuous phase, v the relative velocity between the continuous phase and particle, D_p the diameter of the particle and σ the surface tension between the two phases. The Weber number can be seen on as the likelihood of a particle to undergo break up. If the Weber number exceeds a critical value, this results in a kinetic energy or external force which are said to exceed the strength of the surface tension. The surface tension does no longer manage to hold the particle together, resulting in particle break up. The determination of critical Weber number is a highly discussed process, and different types of break up impacts the value of the critical number. Through his study, A. Wierzba [13] investigated the different ways of calculating and quantifying the critical Weber number, and found through a study of different experiments performed by others that for water particles in air, the critical Weber number was prescribed within the range of 2.2 to 99.6. Multiple ways and expressions for calculating the Weber number was observed. The most common expression, being the same as previously described in equation (3.12). By investigating 25 different methods and reports on critical Weber number, where the majority of the experiments obtained a critical number between 11 and 14, it was concluded that assuming the critical value for water particle break up in air to be $We_{critical} = 12$, is an reasonable assumption.

3.3.2 Brownian motion

Particles of a very small diameter does not necessarily follow Stokes law, but in stead the random motions of Brownian flow. Particles with a diameter smaller

than 0.001 mm, or 1 μm will experience irregular motion and the effect of external forces such as drag force based upon Stokes law is no longer dominating the particle motion and behaviour, and the Cunningham correction factor becomes a important parameter as well as a random acceleration due to the impact of the fluid on the particle.

Due to this random movement, small particles can follow the gas flow, escaping the inertial capturing of the element, but as it passes the element, it might experience some back flow and get captured anyway.

In general, the prediction of these small particles are difficult to perform as random and irregular behaviour is dominating.

3.4 Efficiency

Carpenter and Othmer [7] presented the capture efficiency of a mesh to be a sum of the layers forming the metal foam. In other words, each layer has the same capture efficiency, and the fraction of particles escaping can be written as

$$\xi = 1 - \frac{\eta_{st}}{c} \tag{3.13}$$

where η_{st} is the single target capture efficiency of one wire or fibre, and c a constant presented by Carpenter and Othmer as

$$c = \frac{N_{layers} S_{mesh} h}{F\pi} \tag{3.14}$$

F is a factor measured to be 2/3 and S_{mesh} the specific surface area of the metal foam. Rewriting this equation taking into account the multiple layers within a metal foam, the resulting equation is presented as

$$\xi = (1 - \frac{\eta_{st}}{c})^{N_{layers}} \tag{3.15}$$

The capture efficiency can then be written as 1 - ξ as ξ represents the fraction of particles escaping, not captured.

$$\eta = 1 - \xi = 1 - (1 - \frac{\eta_{st}}{c})^{N_{layers}} \tag{3.16}$$

Inserting (3.14) into (3.16) then gives

$$\eta_{total} = 1 - \xi = 1 - (1 - \frac{\eta_{st}}{N_{layers}} \frac{2}{3} \frac{hS_{mesh}}{\pi})^{N_{layers}} \tag{3.17}$$

This equation describes the efficiency of a fixed mesh.

3.5 Swirling flow

Rotating the metal foam cells does not only introduce a radial movement of the particles, it also introduces a swirling gas and particle flow which is expected to result in vortex or swirling flow.

Within fluid dynamics, a vortex is described as a spinning flow motion around an axis. There are different types of vortices, depending on the vorticity profiles in relation to the distance of the rotating centre- free, forced or combined vortex

Free vortex has a greatest rotational speed at the centre, and the swirling flow decreases as the distance from the centre increases. Forced vortex the swirling is zero at the centre and increases with the distance from the centre.

In a free vortex the tangential velocity is defined as

$$v_{t,radius} = v_{t,wall} \times \frac{r_{wall}}{r} \tag{3.18}$$

where $v_{t,radius}$ and $v_{t,wall}$ is the tangential velocity at a radius r and the wall respectively.

A forced vortex is defined as

$$v_{t,radius} = v_{t,wall} \times \frac{r}{r_{wall}} \tag{3.19}$$

Typically, a solid body rotation introduces a forced vortex type. However, a combination of these two vortex types are also often to be observed, typically within centrifugal separators. Then a free vortex often takes place in the outer parts, close to the wall while a forced vortex takes place in the inner part, this type of vortex is often referred to as Rankine vortex.

3.5.1 Predicted swirling flow within the Lynx Separator

As the rotating element is placed at a certain distance from the inlet, the flow through the cylinder will be affected by this and the size of the angular velocity will influence the outcome of the flow.

If the rotating element introduces a centrifugal force strong enough, a swirling flow might occur already at the inlet, creating a vortex flow with radial movement already before entering the rotating element.

If the centrifugal force does not exceed the drag force at the inlet, this will result in a straight path of flow from the inlet, and the swirling does not take place until the flow reaches the rotating element, hence a radial movement does not take place until inside the metal foam.

3.6 Residence time

Residence time is an expression for the amount of time one particle spends within a system. By this, an overview of the time one captured particle spends in the system in relation to how long one escaping particle spends in the system can be found. Different rotational velocities may result in a reduction or increase for the particle time spent in the separator before escaping or separated. Residence time is also referred to as removal time, and is often used for finding a distribution of reduction in concentration of one fluid relative to the time. The formula of residence time is

$$\tau = \frac{V}{q} \tag{3.20}$$

where τ is the variable for residence time, V is the capacity of the system and q is the flow.

3.7 Sauter Mean Diameter

The Sauter Mean Diameter, d_{32}, is an often used term for average particle size. It is defined as the diameter of a sphere having the same surface area ratio/volume as a particle of interest.

The general term for mean diameter is defined as

$$D_{pq} = [\frac{\int_0^\infty d^p f(d) dd}{\int_0^\infty d^q f(d) dd}] \tag{3.21}$$

where f(d) equals the total number particles integrated from 0 to ∞, giving the Sauter Mean Diameter following expression

$$D_{32} = \frac{\Sigma N_i d_i^3}{\Sigma N_i d_i^2} \tag{3.22}$$

where N_i is the number of particles within the domain.

Chapter 4

Computational Fluid Dynamics

CFD calculations is a well used, but also complex and rather new method for computational calculations of a given problem or situation. Correct computational prediction of fluid flow can contribute to increase efficiency and knowledge, and researching by use of Computational Fluid Dynamics (CFD) has become more and more popular. As the complexity of a system increase and empirical models become hard to use, the tools of CFD becomes quite valuable. CFD is not an option for replacing experiments, but holds several advantages such as cost- and time-effectiveness that can contribute in understanding the behaviour as well as validating the theory.

CFD software uses numerical methods and algorithms to solve and analyse problems within fluid flows. This makes it possible to solve a complex multiphase flow through thousands of iterations. When solving problems with CFD programs, such as ANSYS FLUENT which is used in this thesis, a large number of inputs are available, and considerations must be made when choosing models, solver algorithms and input variables for the specific case study.

This chapter will discuss the equations and theory used when calculating in FLUENT.

4.1 FLUENT solvers

FLUENT has an option of two base solvers, pressure-based models or density-based models. The pressure-based approach was developed for incompressible flows, while the density-based approach is mainly used for compressible flows. In both methods the velocity field is obtained from the momentum equations. The density-based model is not suitable for two-phase flows and would not be accurate for this situation. This limits the simulation of this problem to pressure-based solver.

FLUENT uses finite volume method when discretizing governing equations for continuous and discrete phase.

4.1.1 Conservation of mass

Continuity equation are as follows:

$$\frac{\partial \rho_g}{\partial t} + \nabla(\rho_g \upsilon_g) = 0 \tag{4.1}$$

$$\frac{\partial \rho_l}{\partial t} + \nabla(\rho_l \upsilon_l) = 0 \tag{4.2}$$

for gas phase(g) and liquid phase(l), ρ is the density and υ is the velocity for both phases. The first terms of the equation represents the mass rate increase in time and the second term represents the mass flow out of the control volume.

4.1.2 Momentum conservation

The equation of motion for continuous phase is as described below:

$$\frac{\partial}{\partial t}(\rho \vec{\upsilon}) + \nabla(\rho \vec{\upsilon}\vec{\upsilon}) = -\nabla p + \nabla \vec{\tau} + \rho g + \vec{F} \tag{4.3}$$

which is the Navier-Stokes equation. The first term at the left side represents the momentum increase per time and second term the momentum flux. At the right side the pressure, stress tensor, gravitational force and external forces such as rotational forces are included.

Stress tensor is defined as

$$\vec{\tau} = \mu[(\nabla\vec{v} + (\nabla\vec{v})^T) - \frac{2}{3}\nabla\vec{v}I] \tag{4.4}$$

[1]

4.2 Turbulent $k - \omega$ model

Using the appropriate turbulence model is quite vital for reaching valuable results. The rotational fluid flow makes some turbulent models fail to predict correct results.

Traditionally, the Reynolds Stress Model has been required for calculating high swirling flows. This model also requires high computational power, and the model is quite time consuming in order to fully complete simulations. Lately, the $k - \omega$ model has been proven to give quite similar results, particularly when enabling shear stress tension, SST [2], only to require much less computational power and time than the RSM.

Standard k-ω model solves for kinetic energy k and turbulent frequency ω. This model allows for a more accurate near wall treatment, and performs significantly better under adverse pressure gradient conditions and flows with separation. This model has shown to be quite accurate for wall-bounded boundary layer, free shear and moderate Reynolds number flows. It is suitable for complex boundary layer flows under adverse pressure gradient and separation.

The transport equations for the k-ω model are as presented:

$$\frac{\partial}{\partial t}(\rho k) + \frac{\partial}{\partial x_i}(\rho k u) = \frac{\partial}{\partial x_j}(\Gamma_k \frac{\partial k}{\partial x_j}) + Gk - Y_k + S_k \tag{4.5}$$

$$\frac{\partial}{\partial t}(\rho \omega) + \frac{\partial}{\partial x_i}(\rho \omega u) = \frac{\partial}{\partial x_j}(\Gamma_\omega \frac{\partial \omega}{\partial x_j}) + G_\omega - Y_\omega + D_\omega + S_\omega \tag{4.6}$$

In these equations, G_k represents turbulent kinetic energy, G_ω represents the generation of ω, Γ represents the diffusivity and Y the turbulent dissipation.

4.3 Discrete Phase Model, DPM model

FLUENT allows for simulating a discrete second phase which can consist of spherical particles such as droplets or bubbles dispersed in a continuous phase. The discrete phase follows a Euler-Lagrangian approach where the continuous phase is solved by time-averaged Navier-Stokes equation, while tracking of particles through the flow field solves the dispersed phase. FLUENT computes the trajectories of these discrete entities as well as heat and mass transfer. The discrete particle modelling makes it possible to simulate droplet break up and coalescence. Whenever break up and collision is enabled, FLUENT automatically enables unsteady particle tracking.

Simulating with unsteady problems, the solution in time can be advanced by deciding the desired number of time steps in such a way that particle positions will be updated as the solution advances in time. For an uncoupled flow, the particle position will be updated at the end of each time step, while as for a coupled flow, the positions are iterated on within each time step.

4.3.1 Injection types

FLUENT provides several different types of particle injections, where one of the options are surface injection, where particles are injected from the inlet, one from each face. This way, it is said that the particles are inserted uniformly, spread out over the entire surface. Generally the more particles injected, the more accurate calculation and results,. This also increases the computational time required to complete the calculations.

4.3.2 Particle types

The *inert* particle, represents a particle that obeys the "particle force balance" equation that predicts the trajectory of a discrete phase particle by integrating the force balance on the particle, which is written in a Lagrangian reference frame.

As the droplets may break or coalescence, the diameter of the droplets changes.

4.3.3 Trajectory calculations

The discrete phase solutions is a integration in time of the force balance on the particle. The accuracy of the results is dependant on the time step of the integrations and the coupling between continuous and discrete phases. Integrations of time gives the velocity of the particle in each point along the trajectory.

FLUENT predicts trajectory of discrete phase particles, droplets and bubbles by integrating the force balance on the particles. This force balance equates the particle inertia with the forces acting on the particle, and can be written as

$$\frac{du_p}{dt} = F_D(u - u_p) + \frac{g_x(\rho_p - \rho)}{\rho_p} + F_x \tag{4.7}$$

where $F_D(u - u_p)$ is the drag force per unit particle mass and F_x is an additional acceleration term when operating in an rotating reference frame. The drag force and drag coefficient are determined based on following equations:

$$F_D = \frac{18\mu}{\rho_p d_p^2} \frac{C_D Re}{24} \tag{4.8}$$

$$C_D = a_1 + \frac{a_2}{Re} + \frac{a_3}{Re^2} \tag{4.9}$$

where u is the fluid phase velocity, u_p is the particle velocity, μ is the molecular viscosity, ρ is the fluid density, ρ_p is the density of the particle. a_1, a_2 and a_3 are constants that apply to smooth spherical particles over several ranges of Reynolds number. This drag coefficient is based on the spherical drag model where the shape of the particles is simplified to assuming that they stay spherical. In real situations, the particles may change shape along the flow resulting in a more disk shape as the particles collide, coalesce or break up. This has however not been included here, and the particles are assumed to stay spherical.

Reynolds number is defined as

$$Re = \frac{\rho d_p(\upsilon_p - \upsilon)}{\mu} \tag{4.10}$$

where υ_p and υ is the velocity of the particle and continuous phase respectively.

4.3.4 Droplet collision model

As a part of particle tracking, FLUENT provides an option for estimating the number of droplet collisions throughout the simulation. For any N droplets, they have N-1 options for collision partners, while possible collision partners are $\frac{1}{2}N^2$. The possible collisions is calculated for every time step.

As two droplets collide, the type of collision is determined. Only coalescence and bouncing are possible outcomes considered within FLUENT. The different outcomes can be estimated from the collisional Weber number (We_c), which in FLUENT is calculated from

$$We_c = \frac{\rho U_{rel}^2 \bar{D}}{\sigma} \tag{4.11}$$

where U_{rel} is the relative velocity between two parcels and $\bar{D}$ is the mean diameter of the parcels.

The collision model assumes the frequency of collisions to be of a much smaller value than the particle time step. If the time step of the particle is to large, the results may be time-step-dependant. The collision model is best suited for situations holding small Weber numbers, for a Weber number larger than 100, the collision outcome may be shattering.

4.3.5 Breakup model

FLUENT provides two different breakup models, Taylor Analogy Breakup (TAB) Model and the Wave Model.

The TAB model is best suited for cases where the Weber number is lower than 100, and the Wave Breakup Model is more applicable for higher Weber number giving a more accurate result as the Weber number exceeds 100. This model also requires more computational power and time than the TAB model.

4.4 Rotating frame of reference

For rotating frames of reference, some extra forces are included in the particle trajectories. For rotation about the y-axis, the forces on the particles in x and z

directions is as following

$$(1 - \frac{\rho}{\rho_p})\Omega^2 x + 2\Omega(u_{z,p} - \frac{\rho}{\rho_p} u_z) \tag{4.12}$$

where $u_{z,p}$ and u_z are the particle and fluid velocities in z-direction.

$$(1 - \frac{\rho}{\rho_p})\Omega^2 z + 2\Omega(u_{x,p} - \frac{\rho}{\rho_p} u_x) \tag{4.13}$$

where $u_{x,p}$ and u_x are the particle and fluid velocities in x-direction.

4.5 Steady and transient calculations

When simulating with the Discrete Phase Model (DPM), both steady and transient calculations are an option, as well as steady and unsteady particle tracking. For unsteady simulations, with implicit solvers, the particles are advanced at the end of each time step. Start time and stop time must be specified for transient flows. Injections will start, and stop times set to zero will be injected only at the start of the simulation.

As breakup model is enabled, so is the unsteady particle tracking. If solving for unsteady state continuous phase, particle time step and number of time steps must be inserted, and tracking is performed for every iteration. If steady state discrete phase modelling is used, particles do not interact with each other and are tracked one at a time.

For particle trajectory tracking, the transient state must be enabled, whereas the streamlines of the gas can be view for both steady state and transient state. Performing particle tracking in transient calculations requires all the parameters of the particles to be computed during each time step, and FLUENT saves this information each time. This results in transient simulations not only being more time consuming then steady state, it also results in a large amount of files requiring a high available computational storage space.

Chapter 5

Results and Discussion

5.1 Study case

The results presented in this chapter is based on following case. A small scale model representing the Lynx separator consisting of a cylinder, with three cells representing a microscopic part of a metal foam placed inside. Each of these cells are constructed as a tetrakaidecahedron with 14 facets. Using only a small number of cells for simulations is based on the assumption of the foam consisting of matrices of cells constructed to be completely repeatable and uniform throughout the material [3].

Simulations of air with inert water particles from inlet to outlet of this cylinder is performed in FLUENT. The metal foam cells are set into different angular velocities, implementing a centrifugal force on the system.

For the different angular velocities, the pressure drop from inlet to outlet has been looked into. The radial and axial motion and velocities of the particles, influence of centrifugal force in terms of particle velocity, diameter, particle collision and break up is discussed and the metal foam capture of the different particle sizes are presented.

5.2 Settings

The single tetrakaidecahedron cell has been modelled with a diameter of 0.00275 m. Three cells have been united into one element to represent one metal foam layer. The cells are surrounded by a cylinder with a diameter of 0.01 m and length 0.025 m.

Simulations in FLUENT is performed where turbulent k-ω model with default values is utilized, with both SST and curvature correction enabled. This increases the accuracy of the simulations as the cells are rotating. To include the dispersed water particles, Discrete Phase Model is used, where the two phases are set as interpenetrating media with one-way coupling.

Both air and water particles are set to have a inlet velocity of 10 m/s, and the mass flow rate of the particles is set to 0.003 kg/s. The different particle sizes are 1, 10, 100 and 500 μm, injected uniformly from the inlet surface. Particle collision, coalescence and TAB break up model are enabled, resulting in a diverting particle diameter as the mixture flows through the system.

All walls are set to reflect the flow and all simulations are performed at 288 Kelvin and 1 atmosphere pressure. Gravity of 9.81 m/s^2 is set in opposite direction of the gas flow.

For pressure-velocity coupling, the PISO scheme is utilized and pressure discretization is performed with PRESTO! and first order upwind schemes.

Calculations are run as steady state until convergence before enabling transient state with a time step of 0.001 seconds, performed with 20 iterations per time step.

These settings are further explained in chapter 5.3

5.2.1 Problem setup and geometry

The method used in this thesis for performing simulations in order to evaluate the flow behaviour, has been approached by constructing a single tetrakaidecahedron open cell for calculations in FLUENT. The geometry of the 14 facet tetrakaidecahedron was constructed in ANSYS Mechanical APDL Product Launcher 14.0 where coordinates was inserted and the structure created. The coordinates are

given in Appendix A. These coordinates only constructed the geometry of the cell, not the correct size. Scaling and rounding of the edges has been performed in order to achieve a geometry representing a 10 PPI metal foam by ERG Duocel Aerospace [3]. The typical full sized foam consists of thousands of cells, making one single cell very small. ERG Duocel 10 PPI metal foam holds 5 to 7 cells pr 2 cm, giving a size of approximately 2.8 to 4 mm per cell. Based on this, the diameter of the cells constructed in this case and used for further calculation is 2.8 mm. The diameter of the wires or fibres in the cells are typically with some variation, but around 0.3 mm is a often used size. Three cells have further on been set together representing one layer of cells in a metal foam.

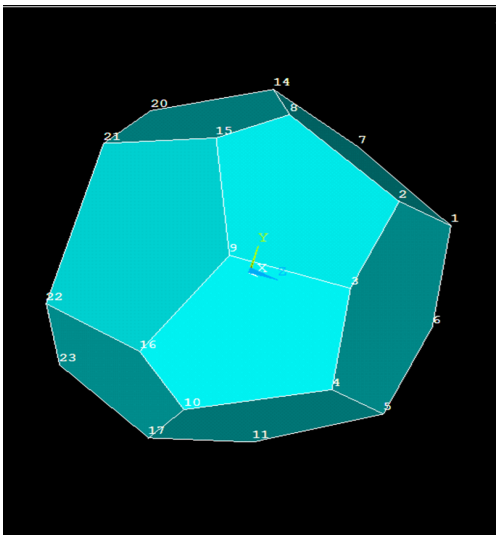

Figure 5.1: Geometry created in Mechanical APDL.

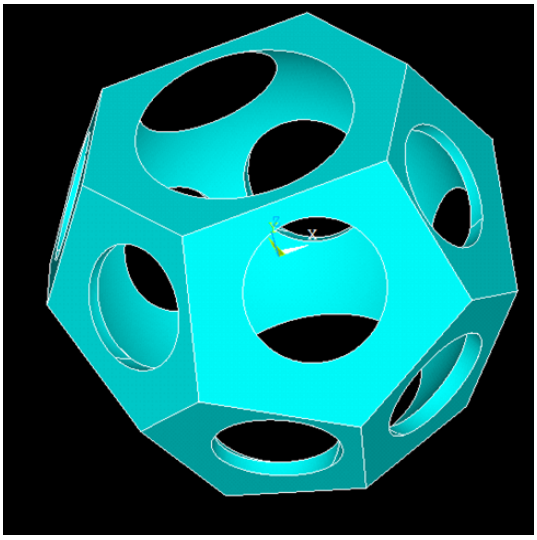

Figure 5.2: Geometry of cell created in Mechanical APDL.

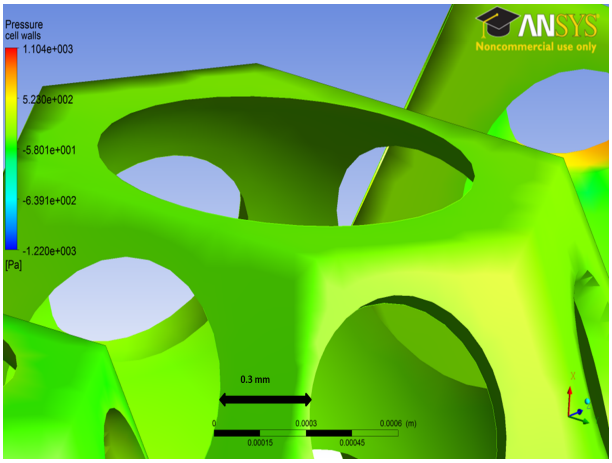

Figure 5.3: Wire size

Due to the small size of the cells, the geometry representing the separator constructed for this case, is rather small. A cylinder with a diameter of 10 mm and 25 mm length of is used for simulations to simulate how gas and liquid parti-

cles of different sizes flow through and interact with the three neighbouring cells representing ERG Duocel metal foam. The separator has been simplified to only consist of a cylinder with a uniform diameter from inlet to outlet.

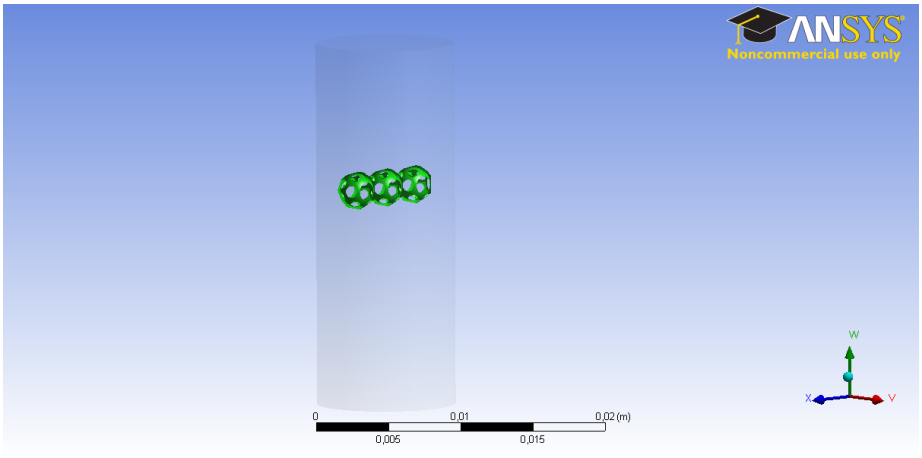

Figure 5.4: Geometry

Parameter	Value	Unit
Cylinder radius	0.005	m
Cylinder length	0.025	m
Cylinder surface area	0.0015517	m^2
Cylinder volume	1.5394×10^{-07}	m^3
Cell diameter (single cell)	2.75×10^{-03}	m
Cell volume (3 cells)	2.9394×10^{-09}	m^3
Cell surface area (3 cells)	6.6864×10^{-05}	m^2
Wire average diameter	3.0×10^{-04}	m
Inlet y-coordinate	-0.015	
Outlet y-coordinate	0.010	
Cell centre y-coordinate	0	
Cell inlet y-coordinate	-0.001375	
Cell outlet y-coordinate	0.001375	
Rotational axis	y	

Table 5.1: Geometrical parameters

5.2.2 Mesh setup

As the geometry of the separator consists of a cylinder and the structure of the cell is quite complicated, the mesh has been set to consist of tetrahedrons, with proximity and curvature sizing. Constructed with 852221 nodes and 617371 elements. This is a quite fine mesh considering the size of the cylinder. Inflation was enabled near the walls and around the interfaces, with a growth rate of 1.2. The inflation layer increases the calculation accuracy close to the wall and boundaries.

Figure 5.5: Cylinder and cell mesh

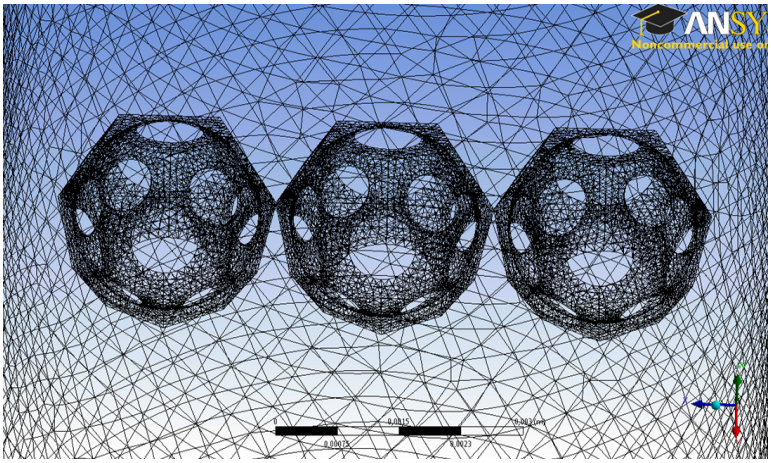

Figure 5.6: Cell mesh

5.2.3 Validation of mesh quality

Validation of the mesh quality is an essential factor for ensuring accurate and stable results. Checking the quality of the mesh was performed based on two different parameters, the orthogonal quality and the cell skewness. Orthogonal quality reports the cell quality, while skewness is defined as the difference between the mesh cell and an equilateral cell of equivalent volume. Highly skewed cells can reduce the accuracy of the solution as well as increase the possibility of calculation divergence.

For the orthogonal quality, a value of 1 represents a good mesh and 0 an unacceptable mesh, while for the skewness this is opposite and 0 represents a good mesh and 1 unacceptable. Low orthogonality and high skewness is therefore not accepted as it will give inaccurate results. Generally, the minimum orthogonal quality should be higher than 0.1 and maximum skewness less than 0.95.

In this case, the minimum orthogonal quality is 0.2302, and the average a value of 0.86, resulting in an acceptable mesh orthogonal quality. The mesh skewness has a maximum of 0.797 which is within the upper level of acceptance, but due to the geometry of the inner cell, reducing this maximum number has showed to be difficult. The average value of the skewness however, is 0.2255 which is a very good value.

5.3 Computational setup

When reaching a certain Reynolds number, the flow becomes unstable and turbulent. The rotating element introduces continuously change in velocity in terms of time and space change, and turbulent modelling becomes essential for running the simulations. As the turbulence introduces unsteady flow, the predictions of flow behaviour becomes difficult, and CFD tools can be very helpful for turbulent cases.

The turbulent model used for all simulations presented is k-ω SST, with default values of k and ω. Curvature correction has been enabled, which increases the accuracy of the streamline curvature and rotational effect on flow trajectories. Including the curvature correction gives results comparable to the Reynold Stress Model, which is proven to be a more accurate model, but one that also requires a higher computational power [2].

All cases has been simulated as steady state and run until converged before enabling transient state. This in order to increase the convergence possibility and reduce computational time. When simulating with a rotational velocity of the cells, steady state will not give good results, and transient simulations becomes essential. Depending on rotational velocity for the cells, the different steady state cases converged between 1000 and 2000 iterations. Number of time steps before converging at transient state showed wider variance than steady state for the different cases. All transient simulations has been performed with 20 iterations per time step. Gravity was enabled in opposite direction of the flow. Each simulation had a simulation time of approximately 10-20 hours before reaching convergence for both steady and transient state.

The working fluids used in the simulations are air and water. Where they are described as interpenetrating continua in such a way that the conservation equations for the different phases are solved separately. One way coupling is enabled. This states that the gas flow can influence the particles, and the fraction of particles are so modest that the particle do not disturb the gas flow.

Parameters	Value	Unit
Gas density (Air) ρ_g	1.225	kg/m^3
Gas viscosity μ_g	1.8×10^{-5}	kg/ms
Particle density (Water) ρ_l	998.8	kg/m^3
Particle viscosity μ_l	1.14×10^{-3}	kg/ms
Surface tension σ	7.35×10^{-2}	N/m
Injected droplet diameter d_p	$1{\times}10^{-6}$	m
	$10{\times}10^{-6}$	m
	$100{\times}10^{-6}$	m
	$500{\times}10^{-6}$	m
Gas velocity inlet	10	m/s
Particle velocity inlet	10	m/s
Rotational velocity of cells	0	rpm
	2000	rpm
	10000	rpm

Table 5.2: Parameters of gas and fluid dynamics

Together with the pressure-based solver, unsteady particle tracking, transient simulation and a mesh consisting of tetrahedrons, the pressure-velocity PISO scheme is said to give the greatest possibility of convergence.

5.3.1 Boundary conditions

The cylinder walls and the cell surface are treated as non-slip boundaries with standard wall functions, this is the default boundary condition in FLUENT. The walls are set to reflect, this ensures the flow to reflect and bounce of the wall as it collides. The inlet is set via velocity-inlet boundary and the outlet flow is set via pressure-outlet boundary. Both the inlet and outlet has defined turbulent specification method as intensity and length scale with 10 %

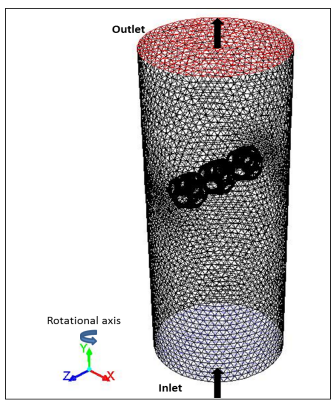

turbulent intensity. At the very inlet the particles have a diameter of 1μm, 10μm 100μm and 500μm. Particle collision, coalescence and TAB break up is enabled for the simulations to become as realistic as possible. The particles are injected with the same velocity as air at the inlet, 10 m/s.

Boundary	Fluent Boundary type
Inlet	Velocity inlet
Outlet	Pressure outlet
Cylinder wall	Wall- reflect
Cell wall	Wall-reflect

Table 5.3: Boundary conditions

Operating conditions	Value	Unit
Temperature	288	K
Pressure	101325	Pa
Specified operating density	1.225	kg/m^3
Time step size	0.0001-0.001	s

Table 5.4: Operating conditions

5.3.2 Model and input validation

Validating the input parameters and the mode settings was done by checking the residuals to be lower than 10^{-3} and evaluating mass flow rate from inlet to outlet. Ideally the difference here should be exactly zero. However, that is rarely the case.

Rotational velocity [rpm]	Δ Mass Flow Rate [kg/s]
0	1.44355×10^{-07}
2000	1.7415732×10^{-07}
10000	3.0483352×10^{-07}

Table 5.5: Difference in mass flow rate from inlet to outlet

For all cases, the differences from inlet to outlet were very small, and they were accepted as ok values.

5.4 Simulation results

The simulations have been run as steady state and transient state, meaning the outcome is time dependant. After having run a large enough amount of iterations, the results stabilized and the solution had come to a seemingly steady state.

Flow of gas and particles are presented by streamlines and track lines respectively, where the results are presented based upon the last time step of the transient state. In all graphics presented in the following chapter, the inlet is coloured by pressure distribution and the outlet is unfilled. As Y[m] is used as a label along x-axis in graphs, it represents the length of the cylinder, from inlet to outlet, where the origin of the cells are at y=0.

5.4.1 Gas flow

The following figures are showing streamlines of the gas flow for the different rotational velocities, 0, 200, 2000 and 10000 rpm of the metal foam cells respectively. This rotational velocity is the only parameter separating the different cases, and it can be seen how increasing the rotational velocity of the cells influences the gas behaviour, where the increase in angular velocity decreases the axial travelling distance before the gas starts swirling.

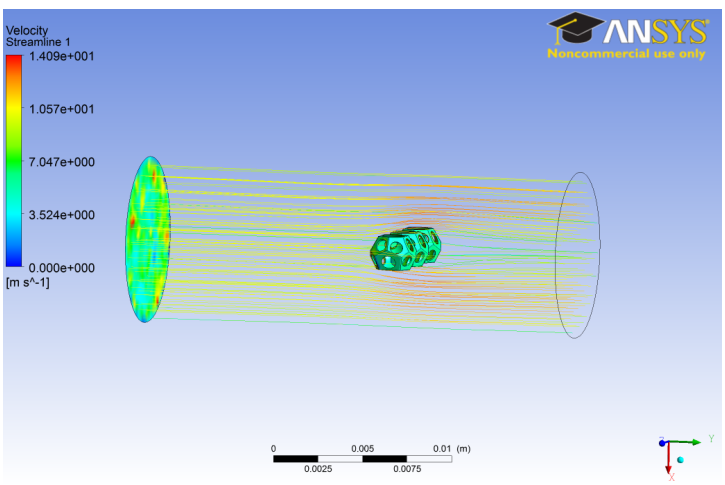

Figure 5.7: Gas streamlines at rotational velocity 0 rpm

With a stationary metal foam, the gas flows linearly without any swirling. As the flow gets closer to the metal foam wires, small movements in the gas streamlines can be observed as the gas flows around the wire obstacles. This is as expected from gas flow physics as described in previous literature. As the gas gets closer to the cells and starts flowing around, an increase in velocity can be noticed. A graphical distribution showing the increase in velocity from selected gas streamlines is included in Appendix B, Figure B.1

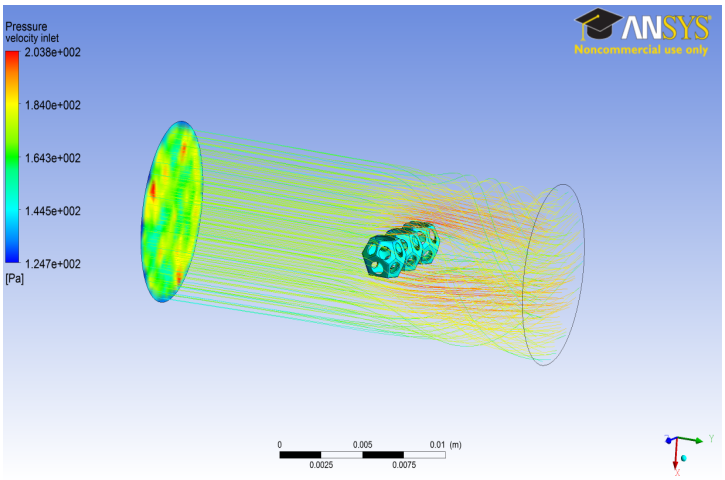

Figure 5.8: Gas streamlines at rotational velocity 200 rpm

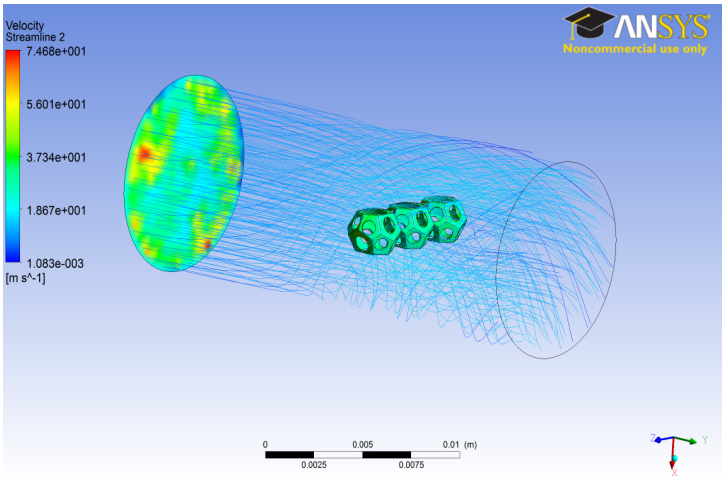

Figure 5.9: Gas streamlines at rotational velocity 2000 rpm

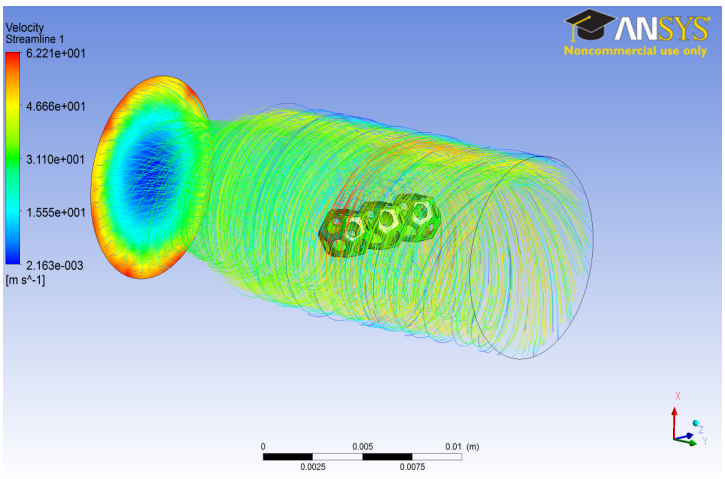

Figure 5.10: Gas streamlines at rotational velocity 10 000 rpm

Rotating the metal foam cells influences the gas flow, and the gas starts to swirl. In the case of 2000 rpm and 200 rpm, the rotation does not affect the gas until it gets close to and passes the cells respectively. Increasing the rotational velocity to 2000 rpm, introduces a swirling gas flow approximately half way between the

inlet and the rotating element, but some swirling tendencies can also be observed quite close to the inlet. Some variety is noticed, where the gas close to the centre of the cylinder flows more straight and the gas close to the wall experiences more swirling, and tendencies of a forced vortex flow can be observed.

Increasing the angular velocity to 10 000 rpm, a swirling gas flow is prominent already at the very inlet of the cylinder. The swirling flow of this case however shows some difference from the other cases, as the gas starts to swirl towards the centre before it starts swirling out towards the walls.

5.4.2 Pressure loss

The metal foam is expected to introduce a pressure loss through the system. Due to the rotation and centrifugal force introducing a tangential velocity in addition to the axial velocity, the prediction of the pressure drop becomes more challenging.

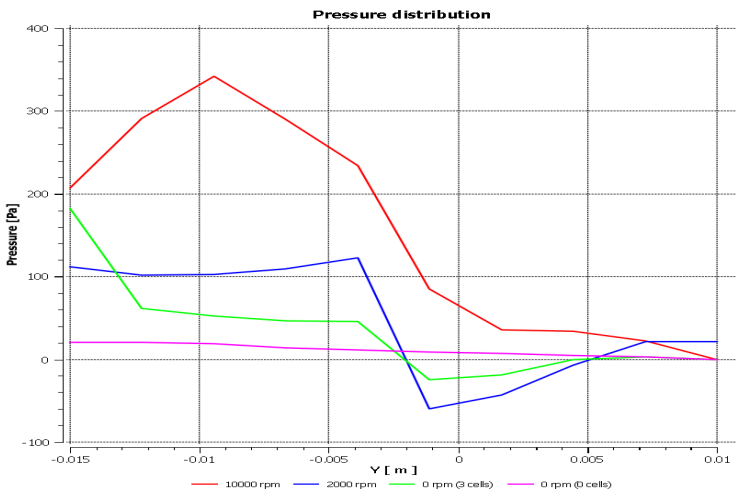

Figure 5.11: Pressure loss from inlet to outlet for different rotational velocities

The figure above shows the pressure distribution from the inlet to the outlet for the different cases presented in the following table. A simulation of only the cylinder without any cells has been run as a reference.

# cells	Rotational velocity [rpm]	ΔP [Pa]
0	0	21
3	0	182
3	2000	90
3	10000	206

Table 5.6: Pressure loss

As seen from the graph, the pressure decreases from inlet to outlet for all cases. The reduction is very small, but due to the size of the system, this is as expected.

To be noticed is that this does not represent the absolute pressure, as FLUENT simulates the absolute pressure as $P_{absolute} = P_{operating} + P_{relative}$, where in this case, the operating pressure is set to 1 atmosphere, and the pressure given at the y-axis of the graph is the relative pressure.

Looking further into the case where the rotational velocity is 10 000 rpm, an increase in velocity is observed before the pressure starts sinking. This is not expected, as one would expect the pressure to only decrease. This might however be a result from the swirling flow that can be observed in Figure 5.10, where the gas is swirling towards the centre of the cylinder before it changes direction and starts swirling towards the walls. A reason for this gas flow behaviour and pressure increase can be that the proposed model is not suitable for this high rotational velocity. This might also be due to the constructed mesh, and a refinement of the mesh could have resulted otherwise, as the inlet is a critical region.

5.5 Particle flow

All particle diameters, 1, 10, 100 and 500 μm are injected with the same mass flow, 0.003 kg/s. This results in a diverting number of injected particles depending on their diameter. The number of particles tracked are however so large, that even for the least number of injections, the amount is assumed to be high enough to give representable results. The range of number of particles injected for the different diameters runs from 5274 to 112926 particles.

The trajectories of particle flow for the different rotational velocities and diameters are included in Appendix B. The graphs presented based upon simulation results given in the following chapter is presented with the ID number of the particles.

5.5.1 Stationary metal foam cells

With a stationary element, hence no centrifugal force present, the drag force and gravitational force are the two dominating particle forces. Based on this, the particles are expected to follow the flow path of the gas, where the smallest particles of 1μm might stay entrained in the gas also when approaching the capturing element, and as the gas flows around the wires, so will the smallest particles. Larger particles has a larger momentum, in such a way that if it is to interfere with the wires, it will collide and not flow past. A change in flow direction and separation from the gas is assumed to take place.

From the trajectories of the smallest particles of 1 microns, it can be seen that they do follow the gas flow, and as they get close to the cells, they flow around following the same path as the gas presented in Figure 5.7.

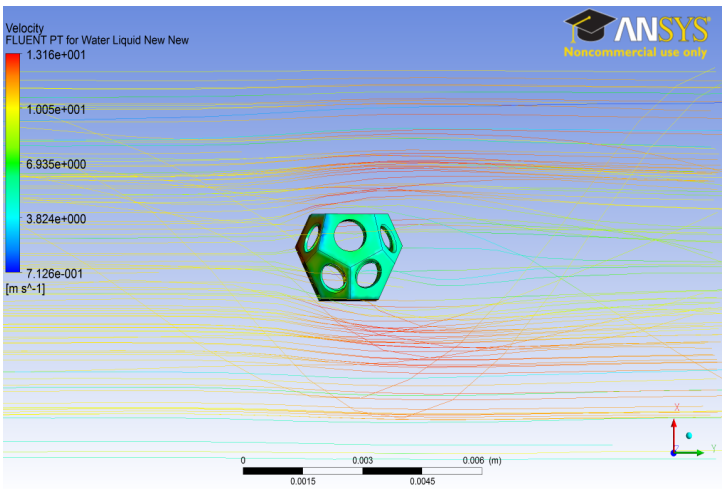

Figure 5.12: Particle flow around cells. 0 rpm, 1 μm

The small portion of particles entering one of the pore openings in the cell, follows the gas flow and change direction with the gas, avoid colliding with the wires. There is however, a very small portion interacting with the wires. The collision does however not seem to impact the flow of these particles enough to separate them from the gas, and the particles continues to follow the gas flow after the collision, escaping further collision with the wires and flowing in a straight line

after exiting the cells. The external forces do not seem to exceed the drag force from the gas.

A closer view of the trajectories of some of these particles are included in Figure B.14 in Appendix B.4.

The collision with the wires results in a small velocity reduction, and the residence time of these particles increases relative to the particles flowing around the capturing element, which in fact experiences a small increase in velocity, resulting in a variation in the residence of these different particles. This is presented in the following figure.

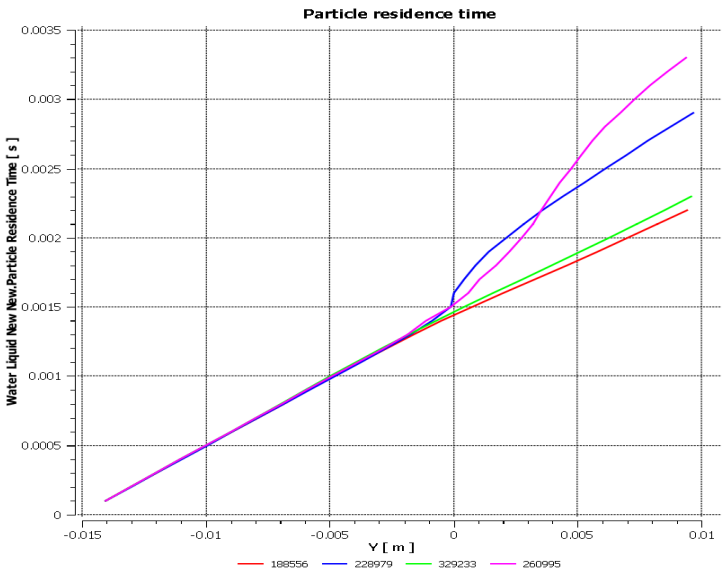

Figure 5.13: Residence time distribution selected particles. 0rpm, 1μm

The two series with the lowest time of residence is flowing around the obstacle, and the two with the highest residence time is flowing through the element. It can be observed that the residence time of the two particles flowing through the element is also quite different, which may be a result from how the particles flow through the cell elements. This does however give a distinct increase in residence time, but it does not result in a radial movement of the particle creating a change in path towards the walls. The impact of the cells is not large enough for these

particles to separate from the gas, and they will exit the system still entrained in the gas flow.

Increasing the particle diameter to 10 μm increases the portion of colliding and collected particles significantly. The interaction with the wires separates the particles from the gas, giving the particles a radial displacement, moving out towards the surrounding wall. This radial displacement is however quite modest, and the particles colliding with the metal foam do not reach the wall before reaching the outlet. In order for these particles to fully separate from the gas and collide with the wall, the particles must be allowed to travel quite a long axial distance after colliding with the cells.

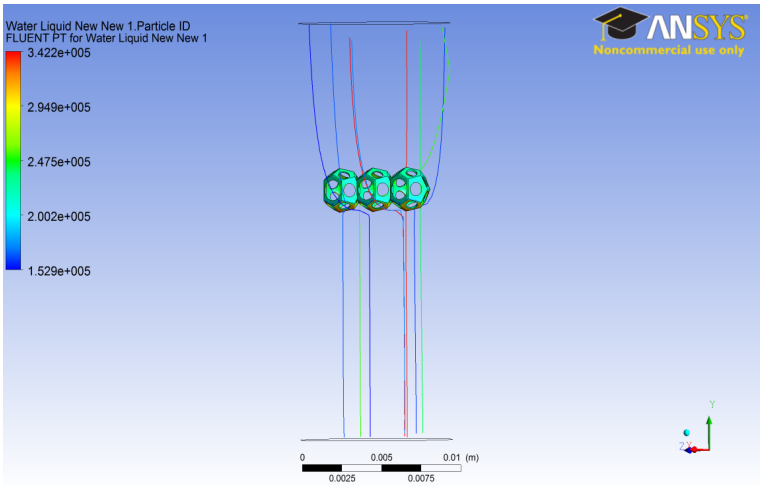

Figure 5.14: Trajectories of selected particles interacting with metal foam cells from inlet(bottom) to outlet(top). 0 rpm, 10 microns

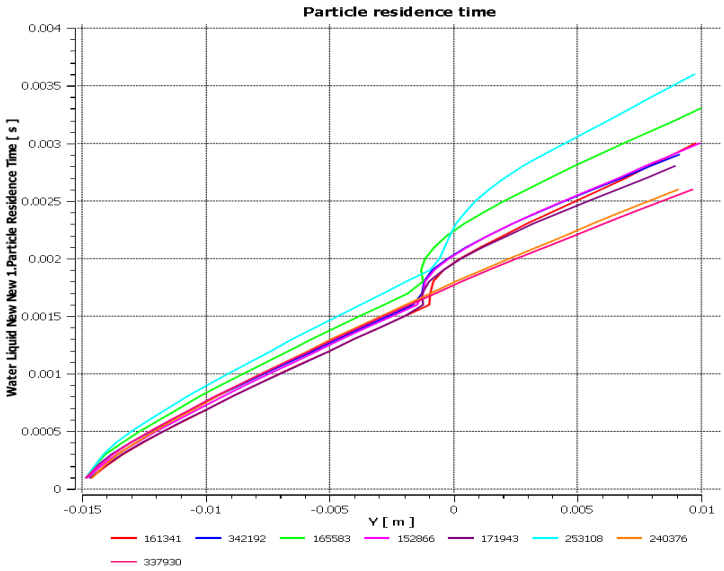

Figure 5.15: Residence time distribution selected particles. 0rpm, 10 microns

The figure presented above shows the residence time for the particles presented in Figure 5.14. The two lower series with the shortest residence time are particles flowing past the metal foam cell without colliding with the wires, while the once above are all interacting with the metal foam. A small variation within the residence time of the colliding particles can be observed, due to where they hit the wire and the path of flow after the collision. The particle with the longest residence time is the only one passing through the metal foam cells, whereas the other hit but do not enter, and instead bounce of and flow around. This is better shown in Figure B.15 in Appendix B.4.

The portion of colliding particles with a diameter of 100 μm and 500 μm are some higher than the smaller particles, but the capturing of these is also very limited. The particles that do collide with the cells, travels a shorter axial distance before reaching the capturing wall, and opposed to the smaller particles, these will separate from the gas. In fact, most move backwards as they hit the wires of the cell, and collides with the wall closer to the inlet than when interacting with the cells. This is presented in Figure B.16.

To be seen from the trajectories of all diameters with a stationary cell element is

how a very small portion of the particles seem as they are experiencing a swirling flow between the inlet and the outlet. This might be a result from particle-particle collisions as this is taken into consideration in the calculations. As two or more particles collide, the might results in a disturbance within the flow. This will be further discussed in section 5.5.5.

5.5.2 Effect of rotation on particles

As the gas starts to swirl with the cells rotating at 2000 rpm, so does the particles. The larger particles, 100 μm and 500 μm quickly flow out towards the surrounding wall. As the diameter of the particles decreases, so does the portion swirling out towards the walls, as many of the particles with a diameter of 1 and 10 microns stay close to the centre of the cylinder, holding a straighter path of flow, hence the interaction with the cells and the capturing of the wires become more important. This can be compared to a regular cyclonic separator where the separation is done by swirling flow. These kind of separators usually are not able to separate smaller particles, typically of a size below 20-10 microns, and this is where metal foam capture becomes an important factor [9].

The critical particle diameter in this case is around 10 microns. Particles with this diameter and smaller are not as influenced by the centrifugal force meaning the drag of the gas flow exceeds the impact of the centrifugal force on the particle. The radial placement of the particles at the inlet seems to determine the swirling in the same way as for those of a larger diameter. The most critical point, and point of interest then becomes the particles with a diameter smaller than 10 microns, entering at a radial position close to the centre of the cylinder. Selecting a group or larger portion of particles to track in FLUENT based upon their radial position at the inlet has not been possible, hence one and one particle must be tracked, making it very time consuming. Due to this, only a small portion of particles are presented.

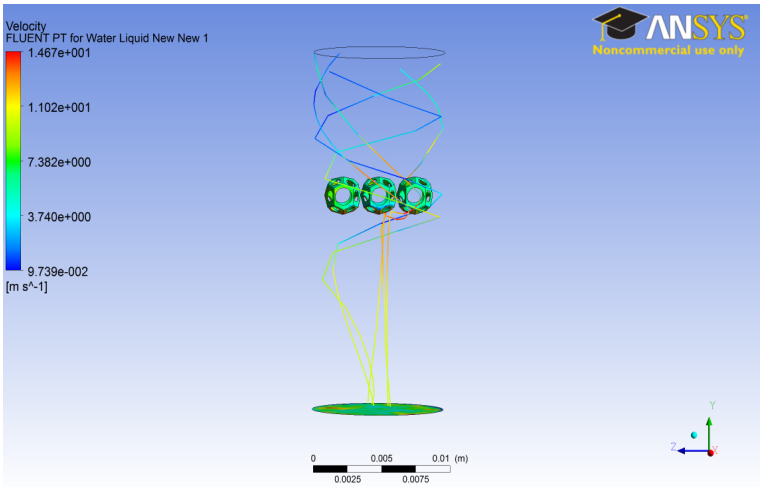

Figure 5.16: 10 μm particles colliding with rotating element, 2000 rpm

The figure above shows a selection of particles of 10 microns, and their trajectories. It can be seen how the influence of the centrifugal force is showing great variance before approaching the rotating element. The particles experiencing swirling flow, hits the wall without interacting with the cells, and the particles flowing at a straight path, collides with the cells, and the swirling becomes a prominent feature after the collision, forcing the particles out towards the walls. Even at approximately the same inlet position, the outcome of the flow can result in variation, making the prediction of the flow hard to perform theoretically.

This increase in rotational velocity then changes the outcome of the 10 μm particles significantly, compared to the case of stationary element. The particles now hit the wall close to the rotating element, hence the axial travelling distance is reduced before hitting the wall, and the separation of these particles can be assumed to be successful.

Based on the given expression for t_{radial}, (3.9), the following table shows a comparison of the same selection of particles from the simulations in FLUENT.

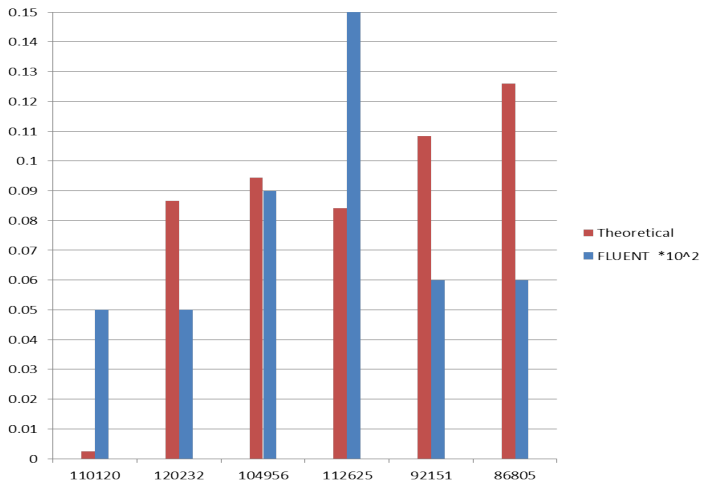

Figure 5.17: t_{radial} for selected particles from FLUENT in comparison with theoretical results from equation 3.9

In Figure 5.17, a diagram showing the time it takes selected particles to radially move towards the walls based upon simulation results and equation (3.9). The results from FLUENT are here multiplied with a value of 10^2, making the particles predicted to move a lot faster by simulations compared to theoretical calculations.

Some notifications must be made upon this comparison. The numerical expression used is a one dimensional expression, whereas the results from FLUENT are three dimensional. The values are taken from a given time the particles reach a given radial distance only in one direction. However, based on this, the results does not support each other. This theoretical model is based upon small particles in the Stokes regime with a small Reynolds number. Due to the centrifugal force introducing swirling and turbulence, this may be a reason for the difference in the results.

Whether the particle flow is dominated by centrifugal force creating swirling, or separated by the collision with the metal foam, gives a distinct velocity difference between the particles. Swirling flow increases the velocity, while flowing through or colliding with the rotating element decreases the velocity. A distribution of the axial velocities is included in Appendix B.4, Figure B.17. For the same particles as presented earlier for 2000 rpm, a distribution of the residence time is given

below.

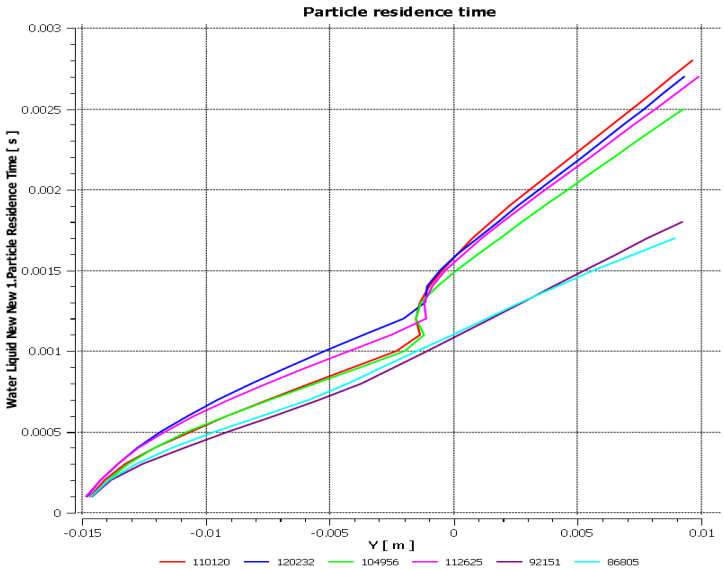

Figure 5.18: Particle residence time. 2000 rpm, 10μm

The two straight lines with the shortest residence time represent the particles swirling out towards the wall, not in contact with the metal foam cells, while the four upper lines represent the particles colliding with the wires. It can be seen how this centrifugal force gives a more distinct division between particles colliding with the metal foam cells, and the particles swirling out towards the walls. Resulting in a difference of 30 %. The swirling flow also reduces the residence time for the particles compared to a stationary case where the particles flow at a straight line from inlet to outlet.

The smallest particles, with a diameter around 1 micron, holds a critical capturing size as they were not captured by a stationary element.There is a small portion of these particles, following the swirling gas, where they hit the wall and as a result of this can be separated from the gas. The majority of these particles however, flows at a straight line without any swirling, and in contrast to the larger particles where collision with the wires introduces a swirling flow at the exit of the rotating element resulting in wall collision, the particles of 1 microns entering the cells or colliding with the wires only shows a small change in radial path of flow, and the

particles do not collide with the wall before approaching the outlet, hence are still not separated from the gas flow.

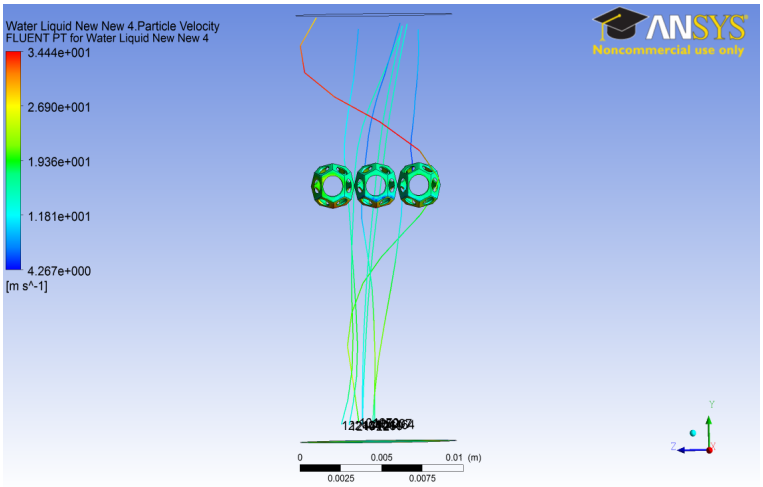

Figure 5.19: Particle trajectories. 2000 rpm, 1μm

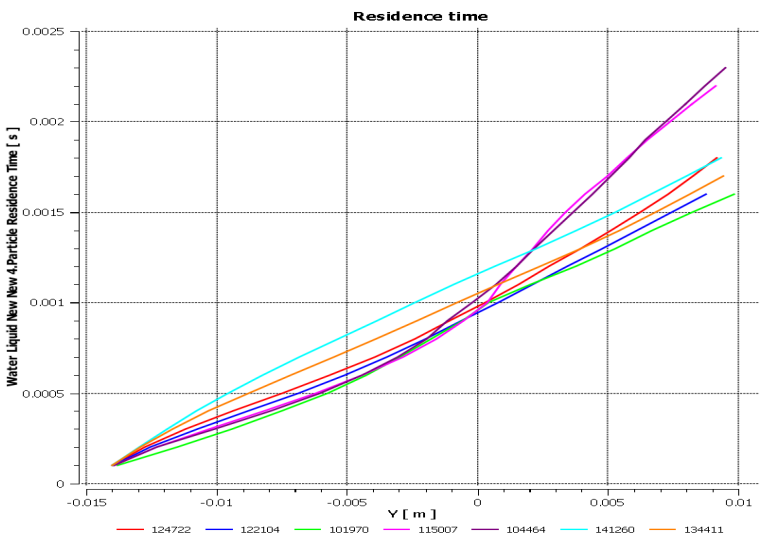

Figure 5.20: Particle residence time. 2000 rpm, 1μm

A small variety in the residence time can be observed for these particles, and similar to the case of 10 microns, the difference between the particles entering and the particles flowing around the obstacle is prominent. However, there is no distinct increase at the very moment of particle-solid interaction as these smaller particles are not as influenced by the solid and the particles does not change direction the same way the larger particles do.

Similar to the stationary situation, only to be more prominent in this case, is how some of the particles start rotating before the gas due to particle collisions. As there is a higher grade of flow disturbances with a centrifugal force present, this can only be expected, and as the larger particles are more influenced by the centrifugal flow and swirling, this can explain why he frequency of this phenomenon is higher for the larger particles than the small.

5.5.3 Weber number

The Weber number increases as the relative velocity between the two phases increases, and is an indication on possibility of particle breakup. Separating the gas and particles from each other by centrifugal force or collision with metal foam wires, introduces a change in relative velocity, and the Weber number follows from this diversity.

As the Weber number is dependant on the particle diameter it is given that a larger diameter will result in a higher Weber number, and larger particles have a higher probability of breaking than smaller. The Weber number can be used as an indication of impact of centrifugal force and metal foam cells for particles holding the same size.

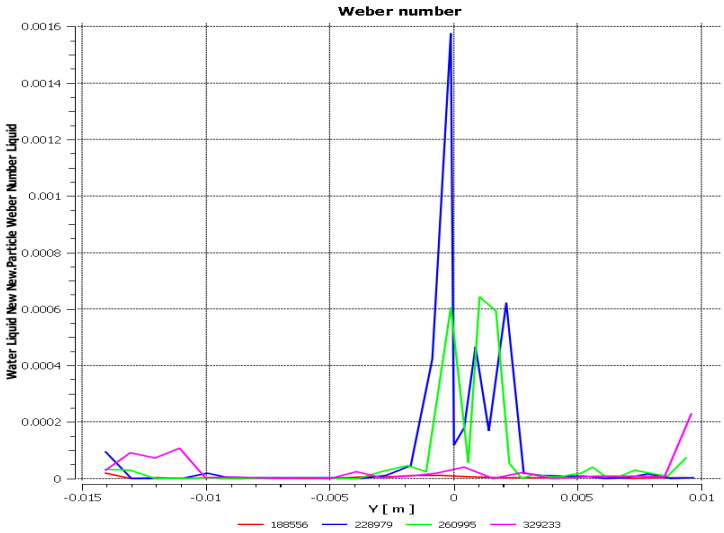

Figure 5.21: Weber number. 0 rpm, 1μm. Trajectories of particles are included in Appendix B.4, Figure B.18

The figure above shows the Weber number for the same particles as previously tracked for a stationary element with a particle diameter of 1μm. The two highest Weber numbers are the two particles presented more closely in Figure B.14, flowing through the metal foam wires. It can be seen that this change in flow direction creates a small velocity difference between the gas and the particles. The highest Weber value is 0.0015, which still is a very low value, and the relative velocity is extremely low.

For comparison, the Weber number of the same size particles, with an angular velocity 2000 rpm is presented below.

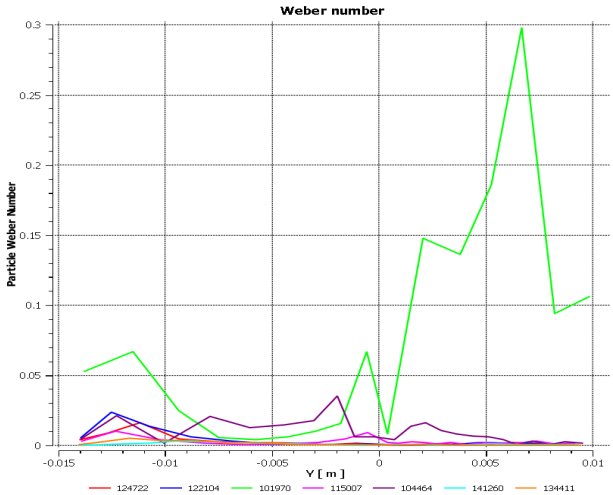

Figure 5.22: Particle Weber number. 2000 rpm, 1 μm

Series 101970 represent the one particle experiencing swirling flow in Figure 5.19.

It can be seen how introducing a centrifugal force and swirling introduces a more disturbing flow where the relative velocity shows greater diversity giving a distinct increase in Weber number.

The inlet of the cylinder becomes a critical point, and as mentioned in previous section, some irregularities was observed for the smallest particles at 2000 rpm, where particle-particle collision seemed to distinguish the flow. The relative velocity does however even out, before approaching the rotating element. An increase in Weber number at the moment of entering the cell can be noticed, but more outstanding is the steep increase after leaving the cells, where the centrifugal force has a higher impact. From this it may be drawn to conclusion that the centrifugal force has higher impact on the particles in terms of creating a relative velocity and increasing the possibility of particle break up then the presence of the metal foam, for the 1 micron particles. The value of the Weber number is still so low that particle break up does not appear.

Increasing the particle diameter to 10 microns, gives a higher impact from the capturing element. Presented below are the Weber number for 10 microns particles at 0 rpm and 2000 rpm.

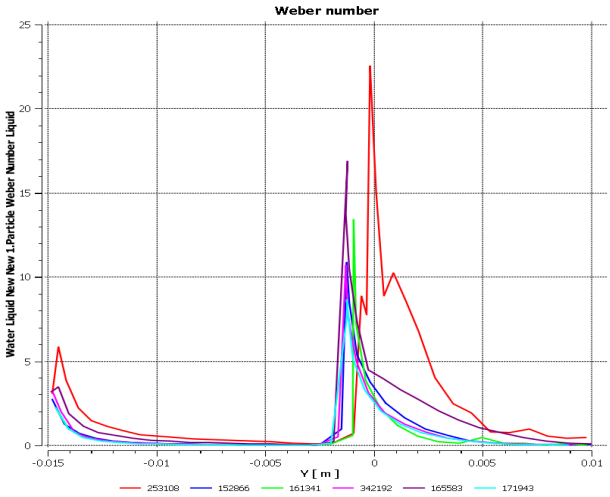

Figure 5.23: Weber number 10 micron particles, 0 rpm. Trajectories of particles are showed in Figure 5.14

Increasing the diameter shows how the collision with the wires causes an instant increase in Weber number, from figure 5.23, to such a high value that break up is predicted to take place.

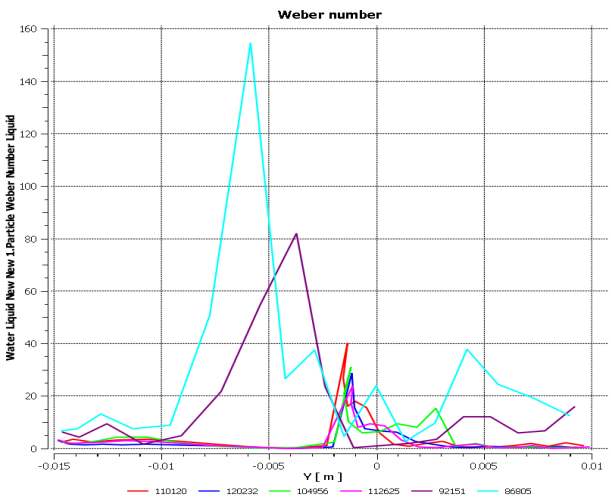

Figure 5.24: Particle Weber number. 2000 rpm, 10 μm

In the case of 10 micron particles at 2000 rpm, the most distinct rise in Weber number is for the two particles under influence of the centrifugal force already at the inlet, flowing in a swirling path, where the peak is representing collision with the wall. The other series, representing the particles flowing at a straight path towards the metal foam cells, and collision with the cells is resulting in a more modest increase in Weber number, but still so high that these particles would break.

With such an increase in Weber number due to the swirling and collision with the wires, a possible outcome, which can not be seen from the simulation results, is that the particles may break into smaller particles before reaching the wall. These new, smaller particles may be so small that they do not get affected by the centrifugal force or captured by the metal foam cells, and follow the gas flow to the outlet of the separator. The capturing from the simulations may then be overestimated, and the efficiency from simulations higher than real life.

5.5.4 Particle velocity

In the following figure, Figure 5.25, an axial velocity profile is presented of the particles at 10 microns with 2000 rpm. From the figure, an instant reduction in axial velocity can be noticed at approximately y = -0.0013 m, which is the moment of collision with the wires.

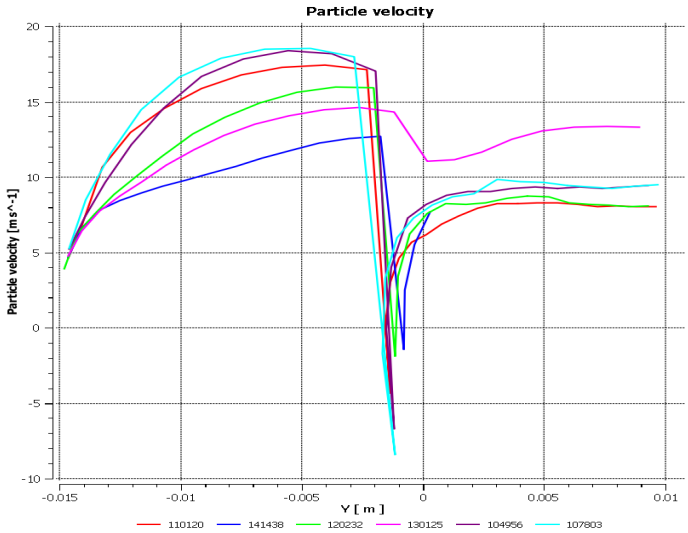

Figure 5.25: Axial velocity profile for particles colliding with the aluminum wires. 2000 rpm, 10μm

The series showing 130125, with a smaller velocity reduction is representing a particle flowing through the cell without any contact with the wires. It is showing a quite prominent axial reduction even without colliding with the cell wires.

For the same particles, the figure below is showing the radial velocity due to the collision with the cell wires. The particles are flowing at a relative constant radial velocity before interacting with the wires where it increases quite rapidly. The particles collides with the wall at the peak of the graphs, where one can see that the particles does not move much in the axial direction compared to radial movement before colliding with the wall, where it ideally will be captured.

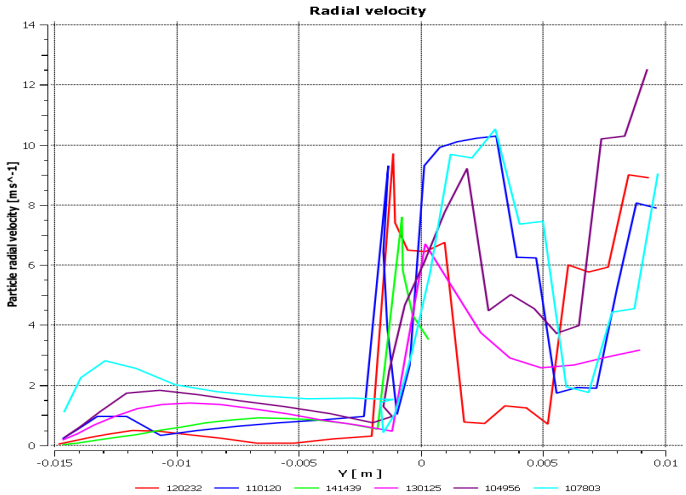

Figure 5.26: Radial velocity profile for particles colliding with the aluminum wires. 2000 rpm, 10 μm

For comparison, a distribution showing the axial velocity of particles not colliding with the capturing element is presented below.

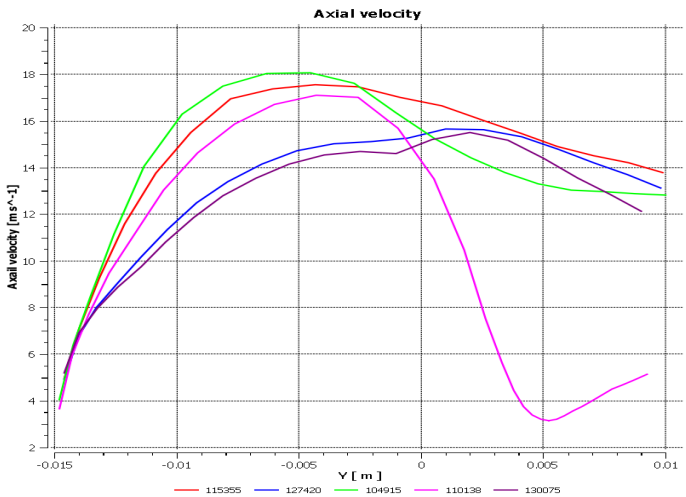

Figure 5.27: Axial velocity particles flowing around the metal foam cells. 2000 rpm, 10 μm

5.5.5 Particle diameter

At the inlet, the particles are injected as 1, 10, 100 and 500 μm, with a diameter distribution set as uniform. However, as the collision model with coalescence and break up is enabled, the diameter of the particles are changing as they flow through the cylinder. By investigating the Sauter Mean Diameter, the diameter increase or decrease through the system for the different inlet diameters can be found.

In the following figure, a distribution showing the percentage diameter growth is presented.

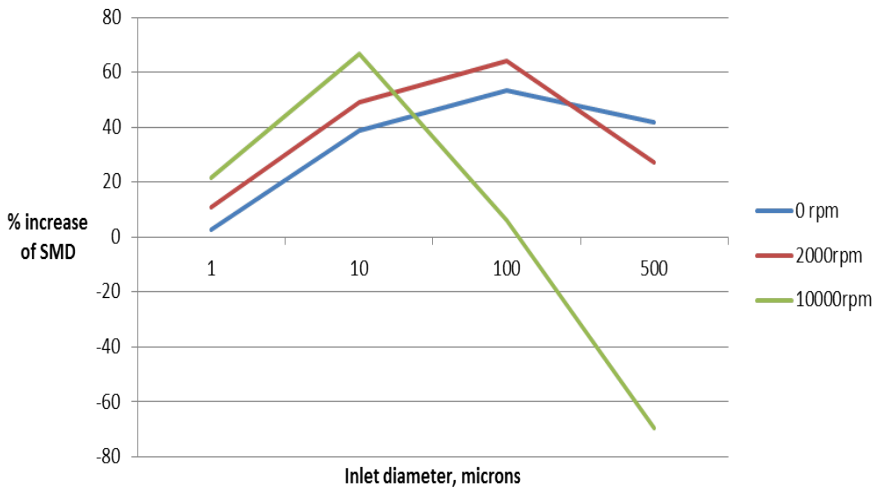

Figure 5.28: Increase of mean particle diameter.

From this it can be seen that the rate of coalescence of particles increases with particle inlet diameter and angular velocity. This until a critical diameter and rotational velocity is reached, and the coalescing is not as prominent any more. As the centrifugal force has greater impact on the larger particles than the smaller, and the swirling causes disturbances in the flow, the outcome of this can be a higher portion of particle-particle collision and coalescence for these larger particles. However, this swirling also introduces wall collision which contributes in particle breakup. The Weber number has showed to increase for increasing ro-

tational velocity and particle diameter, indicating an increase in particle break up.

This can describe the reduction in Sauter Diameter for the particles of 500 microns, where particle break up becomes more prominent and the mean diameter decreases as the angular velocity increases. Especially when increasing to 10000 rpm, where the mean diameter becomes close to 70% lower than the inlet diameter. These results are however presented with uncertainty as this high rotational velocity has shown to reduce the reliability of the model.

Increasing the angular to such a high value that the rate of particle break up exceeds the rate of coalescence might decrease the efficiency and capture from the metal foams as these particles split into smaller particles which may be more difficult to capture.

In the case of 100 microns, the coalescence is more prominent for 2000 rpm, and the break up rate increases when increasing to 10000 rpm, but it is still a higher diameter than at the inlet, and the coalescing rate is still the dominant feature.

To be noticed, all particle sizes are injected with the same mass flow. Meaning the number of injected particles are higher for smaller particles than larger particles, and one could expect the number of collisions and coalescence rate to be higher for these small particles as there are more particles to collide with, giving a higher increase in Sauter Diameter. In the case of a stationary element, this could have been expected.

For the 10μm particles, which by the trajectories experienced both swirling due to the centrifugal force and a straighter path of flow in the centre towards the capturing rotating element, it can be concluded that the collision with the rotating element and the swirling does not influence these particles enough for the rate of particle break up to oversee the coalescence rate. The same goes for the smallest particles, where the increase in angular velocity contributes to an increase in Sauter Mean Diameter, and a higher rate of coalescence takes place for these particles.

All particles larger than 1 microns have quite a high increase in mean diameter when the metal foam cells are held stationary. This can explain how it might look like a small portion of the particles are swirling even if there is no centrifugal force present. This particle motion is a result of particle-particle collision and coalescence.

5.5.6 10 000 rpm

Increasing the rotational velocity resulted in failure regarding the particle tracking. There are almost no particle track lines completed from inlet to outlet. The model seems to complete the streamlines of the gas flow, but not the particles. This could have resulted otherwise if using RSM model which is better suited for high rotations, or enabling wave break up model which might be more accurate for higher Weber numbers. Reducing the size of the time steps has been attempted, resulting in incomplete calculation and computational crash. This could however increase the tracking of the particles.

5.6 Limitations and weaknesses of proposed model

CFD models and simulations run on a normal laptop are often simplified, and can in most cases be modified into becoming more accurate and more applicable to real life situations. In order to increase accuracy, testing must be performed, and simulations must be run with different inputs, models and results must be tested upon. This is a very time consuming process, and limitations are normally set regarding available time, computational power and available storage space. Several attempts on increasing the resemblance to real life geometry and structure has been made during the process of this modelling, resulting in computer crash, and the limitations in time and power did not allow for more simulations to complete than those presented in this thesis.

In many cases, the default values in FLUENT works ok. It can also be very helpful in cases where one does not know all input parameters. FLUENT then makes it possible to reach a good result when performing enough iterations. Using default values does not ensure converging results, and many values needs to be evaluated in order for the calculations to converge. As input values are changed, so is the possibility to convergence.

In this case, the relaxation factors has been increased to increase the possible convergence during calculations. PISO algorithm for pressure-velocity coupling with first order implicit formulation for unsteady integration at first order upwind scheme discretization has been used. Higher order terms are however to be preferred as they give a more accurate solution. As the order of schemes increases, so does the difficulty for achieving convergence. If convergence is not reached, the

results are useless. In this case, second order schemes failed to give a converged result as simulations could not be completed.

Enabling collision with coalescence and break up ensures the simulations to be more realistic. This also makes the flow more complex and a higher rate of disturbance within the flow is a result of this. With the rotational velocity present for this study, coalescing and break up has showed to be a prominent feature, and this should be a part of the simulations for the results to be realistic. However, this creates a high variation in particle diameter, making the tracking of particles with the exact same diameter difficult. For the different graphs given in the results, particles presented has been chosen with caution. The particles presenting 10 microns, are however within the range of 1.0×10^{-5}m and 1.3×10^{-5}m, which may affect the results. The smallest particles injected as 1 microns, showed a smaller rate of coalescing and break up, and the particles presented for comparisons are all with a diameter of 1 micron.

Tracking particles from their trajectories can be challenging. The track lines are based upon the origin of the particle, and as it might seem from the track lines that the particle is colliding with the solid, it is unknown how large portion of the particle actually colliding.

Two of the main attempts made in this thesis for improvements for increasing the resemblance to real life is changing the boundary conditions of the surrounding wall to *trap* instead of *reflect*, and creating an opening in the wall around the rotating element, allowing the particles to escape is also an option. Doing so, may increase the possibility of reliable results regarding the total efficiency of the separator as well as the overall behaviour of the flow.

Chapter 6

Conclusion

A simple, small scale model of the Lynx separator for calculating gas-liquid flow in ANSYS FLUENT is proposed. Turbulent k-ω model with curvature correction is used in combination with the Discrete Phase Model to simulate flow of air with inert water particles with a diameter range from 1 μm to 500 μm. A capturing element is placed in a cylinder constructed as three tetrakaidecahedron cells representing a microscopic 10 PPI open pore metal foam from ERG Duocel. This element is set into different rotational velocities to investigate the influence of this on the particles.

The simulations showed that the proposed model is able to predict the impact of the centrifugal force as well as the metal foam cells on the different phases as long as the angular velocity holds a moderate value.

The results presented and conclusions drawn in this chapter are only based on the exact cases simulated in this project, and does not necessarily hold in general or in real situations.

With a stationary cell element, both the gas and the particles flows at a straight line from inlet towards outlet, where as the gas reaches the metal foam element, it flows around it. The 1 micron particles are following the gas flow, also when reaching the cells, and they flow around the obstacle, escaping colliding with the cells. The larger particles, follows the path of the gas towards the metal foam cells, but as the gas and smallest particles flow around, the larger particles collides with the wires, creating a disturbance in the flow path, forcing them to bounce of the

element and flow around towards the outlet or the wall, depending on the particle size. The larger the diameter, the larger the fraction of colliding particles, and the shorter axial travelling distance before colliding with the wall. The fraction of the largest particles colliding are still limited and the majority of the particles flow through the cells rather than colliding.

Introducing an angular velocity to the metal foam cells, with a rotation of 2000 rpm, gives a swirling flow of the gas as well as the largest particles. As the particles swirl out towards the wall, they do not interact with the rotating element, and the centrifugal force becomes the main separation mechanism for both 100 μm and 500 μm. The 10 μm are experiencing a combination of swirling flow and a more straight flow, where it is drawn to conclusion that the radial inlet position impacts the outcome of the flow. The capturing of the cells flowing straight is quite good and the majority of the particles flowing towards the cells are colliding with the wires, giving a radial displacement resulting in wall collision. Only a limited portion of the smallest particles with a diameter of 1 μm is swirling out towards the walls, as most is flowing in the centre, and the centrifugal force can be concluded to have a very little influence on these particles. They are not captured by the rotating element, and the radial movement of these particles are so small they reach the outlet before reaching the wall.

The largest particles are captured by the presence of the metal foam cells already when the element is held stationary. Introducing a centrifugal force gives a swirling flow for the larger particles, forcing them out towards the wall before reaching the rotating element. This is advantageous as this limits the hold up of larger water particles at the wires of the element, increasing the chance of capturing the smaller particles.

Interaction with the metal foam cells has several outcomes and scenarios depending on the diameter of the particles:

- 1 μm particles colliding continues to flow through the cells with a minimum radial displacement, with both a stationary and rotating element. The separation of 1 micron particles has in general showed to be minimal as these particles follows the gas stream.
- 10 μm particles colliding bounce of and flow around the cells and towards the outlet with a axial and radial movement. There is a high increase in metal foam cell impact on these particles from stationary element to 2000 rpm.

- Collision with the wires for particles 100 microns or larger results in the particles bouncing of the wires and flowing in opposite direction of the flow before hitting the wall.
- Entering the cells does not implement a radial movement. The collisions with the wires determines the outcome of the movement.
- As the smallest particles entrained in gas flows around the wires avoiding collision, an increase in axial velocity for both gas and particles is observed.
- Particles entering the cells and flowing through has a decrease in axial velocity even if not colliding with the wires.
- Larger particles swirl out towards the surrounding wall under greater influence of the centrifugal force, while 1 microns and 10 microns particles stay closer to the centre of the cylinder.
- The centrifugal force becomes prominent already before reaching the rotating element, not only after.
- The main separation mechanism of 100 μm and 500 μm is the centrifugal force. This is advantageous as they do not collide with the metal foam, and the smaller particles can get captured instead.
- The Weber number increases with the diameter of the particles and the angular velocity of the rotating element.
- The collision with 1 microns and 10 microns and the stationary element does not increase the Weber number to such a high value that particle break up can be expected.
- Increasing rotational velocity decreases the amount of larger particles colliding with the element as they flow out towards the walls before approaching the rotating element

Investigating the Sauter Mean Diameter showed that for 1 μm and 10 μm particles, the portion of particles breaking is limited and coalescence is the dominating collision outcome. This is an advantageous, as larger particles are more easily captured and separated.

The larger particles are more influenced by the centrifugal force, experiencing a higher rate of collision, especially with the wall, and particle break up becomes more relevant.

For the largest particles injected, the highest rotational velocity results in a reduction of Sauter Mean Diameter of 70% relative to particle inlet diameter. The reliability of this results is however unknown, as this high rotational velocity may not be suitable for proposed model.

Increasing the angular velocity og the rotating element should be done with caution as this has shown to increase particle break up for larger particles, resulting in creation of smaller particles which has shown to be more difficult to capture and separate from the gas.

This model has show to perform badly for very high rotational velocity in terms of particle tracking and pressure distribution. The increase from 2000 rpm to 10000 rpm is however large, and at what exact angular velocity the reliability of this proposed model starts sinking, is unknown.

6.1 Further work

In order for this model to be fully validated, there are several aspects that should be looked further into. The simulations should, if computational power is available, be performed with Reynolds Stress Model as this is better suited for highly rotational flows, and verifications should be made for the different models comparing the results.

In terms of increasing the rotational velocity, the proposed model should be improved, and suggestions are to perform simulations with RSM and Wave Break up model.

Experiments should be run for better validation of the model and results, but also in order to increase the knowledge on how to use this microscopic model in relation to real size situations.

As of now, the proposed model is quite time consuming in terms of completing calculations. Ideally, the models should be as computationally inexpensive as possible, giving this model room for improvements. As higher order terms are to be preferred during calculations, this will contribute to increasing the computational time even more, and optimization of proposed model is suggested. The mesh used is quite fine and the number of elements is high relative to the size of the system. Ideally, the mesh should be as course as possible without this affecting

the accuracy and results. A refinement of the mesh can be proposed in order to reduce the simulation time and power consumption.

The geometry of the metal foam cells can be improved as the wires or fibres in the cell can be constructed as more cylindrical. This might change how the particles flow after colliding with the wires. The surrounding wall of the cylinder should be simulated as a trap instead of reflecting to get a better overview of the efficiency and increasing the similarity to real life.

Bibliography

[1] *ANSYS FLUENT Theory Guide.*

[2] *ANSYS FLUENT User's Guide.*

[3] ERG Materials & Aerospace. https://www.ergaerospace.com. Accessed: 15/04/2013.

[4] Louis E.Stein Alex C.Hoffmann. *Gas Cyclones and Swirl Tubes.* Springer-Verlag Berlin Heidelberg, 2008.

[5] Statoil RD Center Bernt Henning Rusten. Gas/liquid separation, October 2012.

[6] Bert Brouwers. Rotating particle separator: A new method for separating fine particles and mist from gases. *Chem. Eng. Technol*, 1996.

[7] Donald F. Othmer C. LeRoy Carpenter. Entrainment removal by a wire-mesh separator. *A.I.Ch.E. Journal*, 1955.

[8] Richard Holdich. *Fundamentals of Particle Technology.* Midland Information Technology and Publishing, 2002.

[9] Mueller Environmental Designs Inc. Fundamentals of gas solids/liquids separation.

[10] S.Y. Kim J.M Hyun J.W. Paek, B.H. Kang. Effective thermal conductivity and permeability of aluminum foam materials. *International Journal of Thermophysics*, 2000.

[11] Gisle Otto Tviberg Monsen. Modeling of a centrifugal separator for dispersed gas-liquid flows. Master's thesis, NTNU, 2012.

[12] Bhavani V. Sankar Nagaraj K. Arakere Prasanna Thiyagasundaram, Junqiang Wang. Fracture toughness of foams with tetrakaidecahedral unit cells using finite element based micromechanics. *Engineering Fracture Mechanics*, 2011.

[13] A. Wierzba. Deformation and breakup of liquid drops in a gas stream at nearly critical weber numbers. *Experiments in Fluids*, 1990.

Appendix A

Coordinates of tetrakaidecahedron

VERTEX	X	Y	Z
V1	2	0	4
V2	0	2	4
V3	-2	0	4
V4	-2	-2	4
V5	4	0	2
V6	0	4	2
V7	-4	0	2
V8	0	-4	2
V9	4	2	0
V10	2	4	0
V11	-2	4	0
V12	-4	2	0
V13	-4	-2	0
V14	-2	-4	0
V15	2	-4	0

V16	4	0	-2
V18	0	4	-2
V19	-4	0	-2
V20	0	-4	-2
V21	2	0	-4
V22	0	2	-4
V23	-2	0	-4
V24	-2	-2	-4

Table A.1: Tetrakaidecahedron-Lord Kelvin's Solid

Appendix B

Gas and particle tracking

B.1 Gas

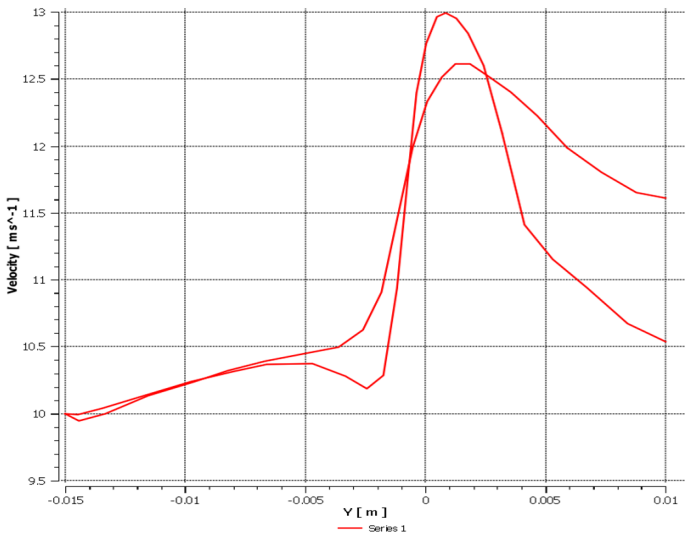

Figure B.1: Gas velocity 0 rpm

Particles

B.2 0 rpm

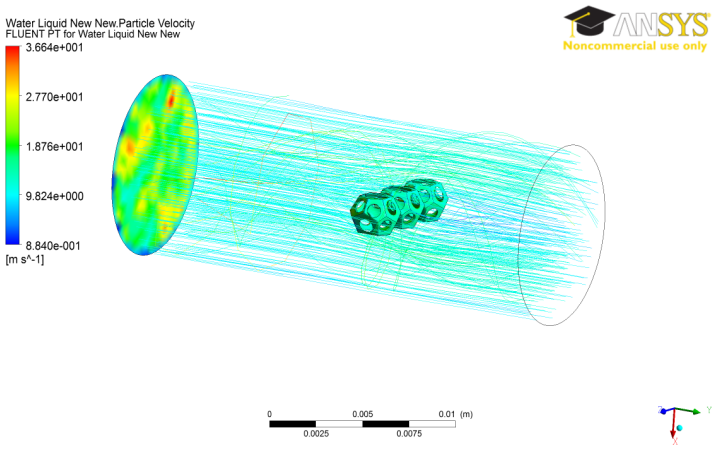

Figure B.2: Particle track lines, 0rpm-1 microns

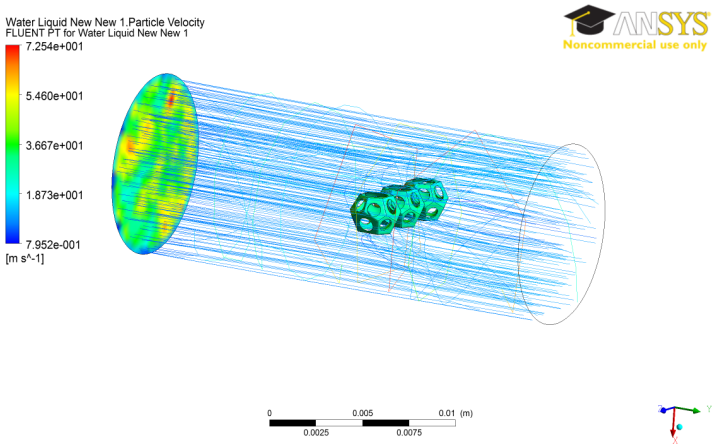

Figure B.3: Particle track lines, 0rpm-10 microns

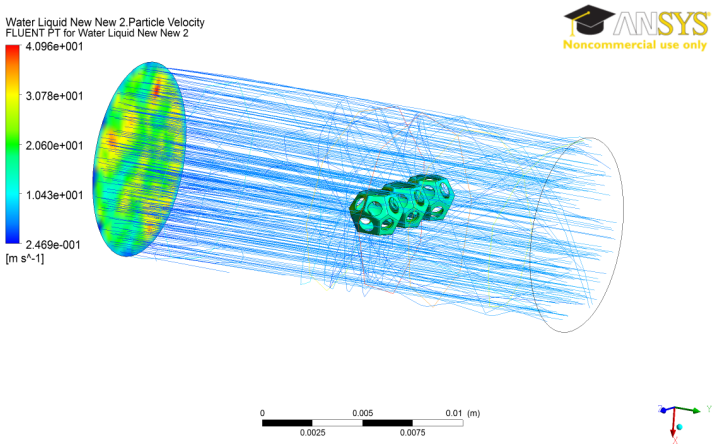

Figure B.4: Particle track lines, 0rpm-100 microns

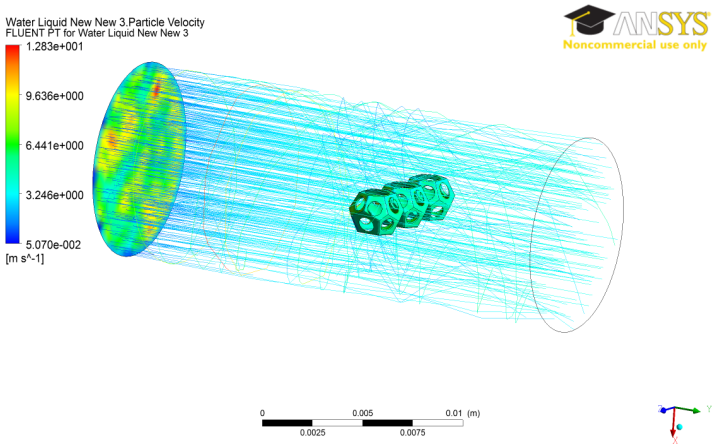

Figure B.5: Particle track lines, 0rpm-500 microns

B.3 2000 rpm

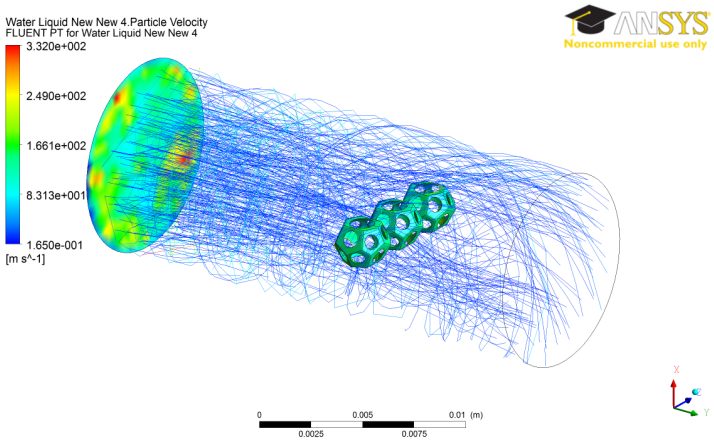

Figure B.6: Particle track lines, 2000rpm-1 microns

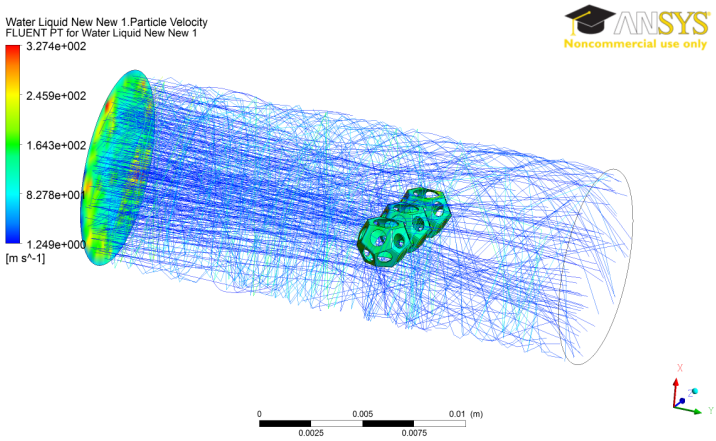

Figure B.7: Particle track lines, 2000rpm-10 microns

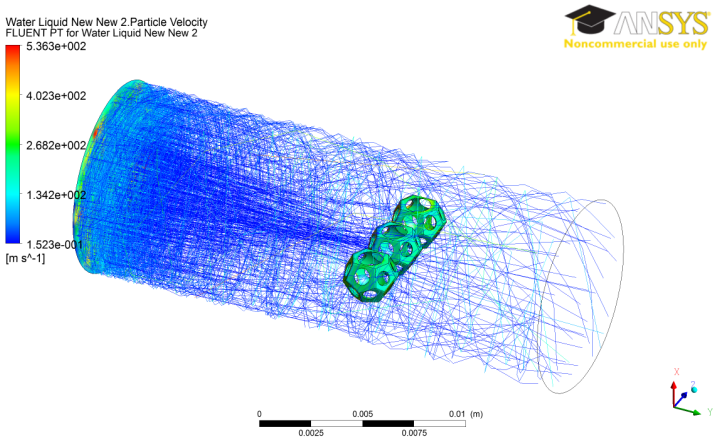

Figure B.8: Particle track lines, 2000rpm-100 microns

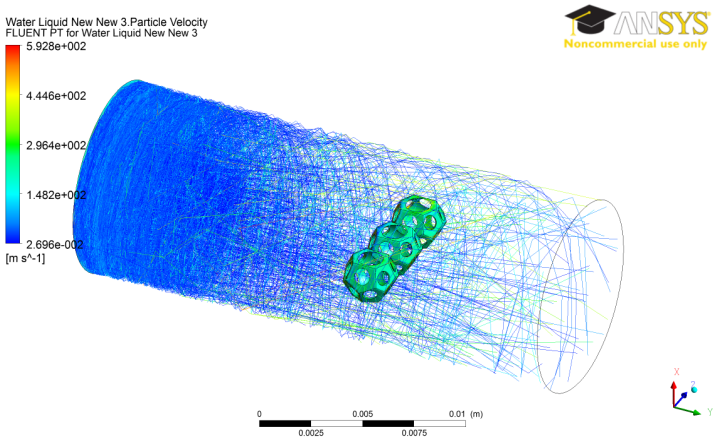

Figure B.9: Particle track lines, 2000rpm-500 microns

B.4 10000 rpm

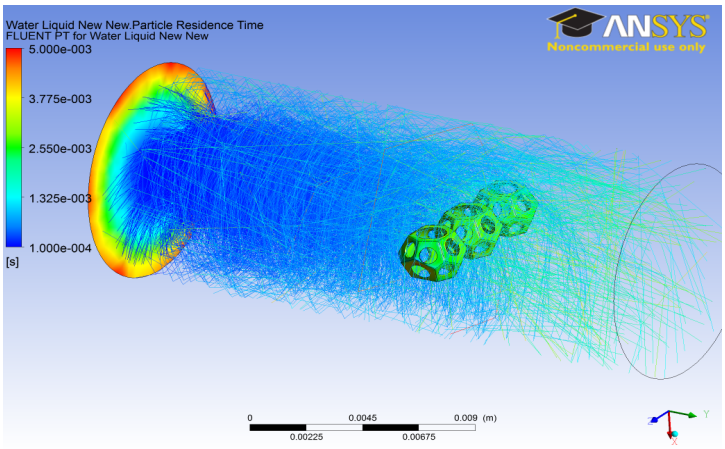

Figure B.10: Particle track lines, 10000rpm-1 microns

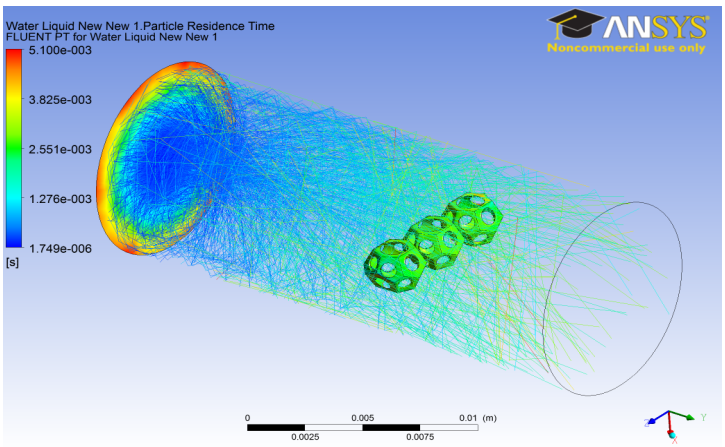

Figure B.11: Particle track lines, 10000rpm-10 microns

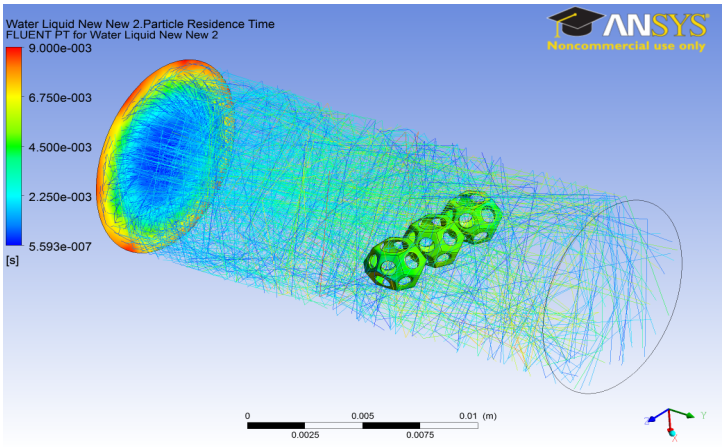

Figure B.12: Particle track lines, 10000rpm-100 microns

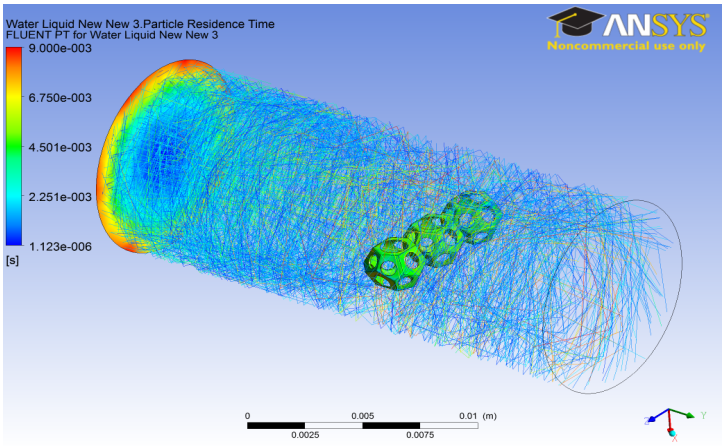

Figure B.13: Particle track lines, 10000rpm-500 microns

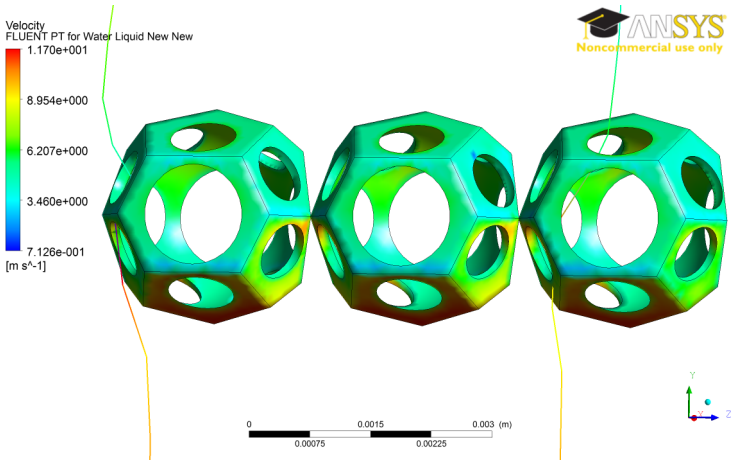

Figure B.14: Particle track lines showing how particles flow around the wires escaping capture. 0rpm, 1 μm

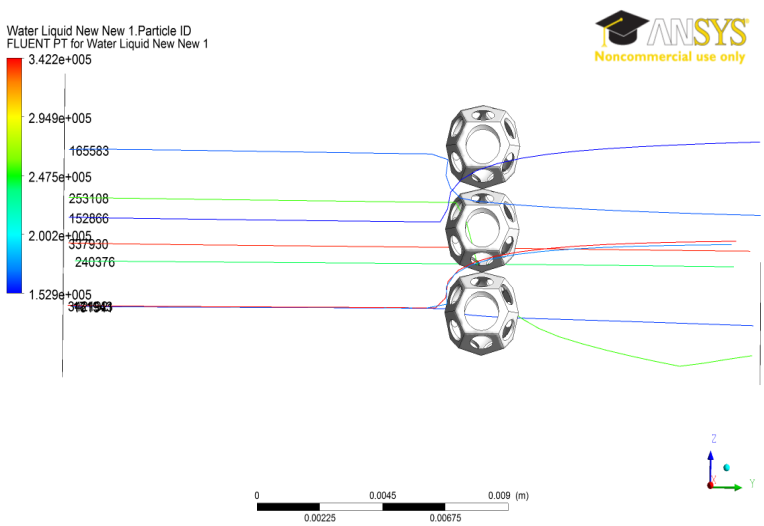

Figure B.15: Particle track lines, 0rpm-10 microns

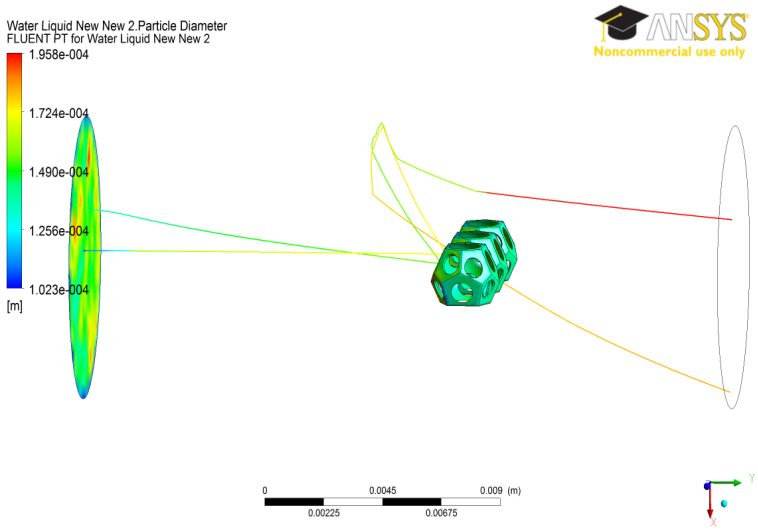

Figure B.16: Particles colliding with cells, 0rpm-100 microns

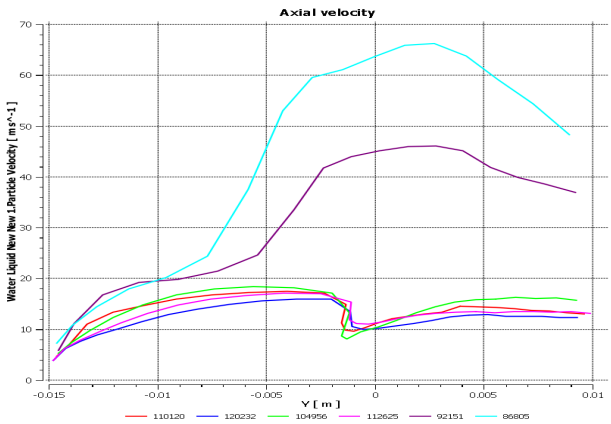

Figure B.17: Axial velocity distribution for selected particles

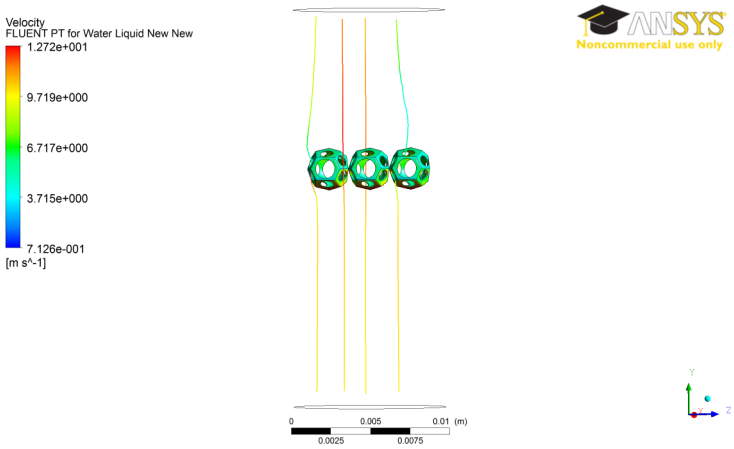

Figure B.18: Particles used for Weber number distribution in Figure 5.21. 0 rpm, 1 micron

Appendix C

FLUENT settings

Category	Subcategory	Choice
General	Solver type	Pressure-based
	Time	Steady, Transient
Models	Model	SST k-omega
	Options	Curvature correction
	Constants	Default values
	Gravitational acceleration	x=0, y=-9.81, z=0
	Model	Discrete Phase Model
	Options	Interaction with continuous phase
		Unsteady particle tracking
		Track fluid flow every time step
	Tracking	Max number of steps- 50000
		Drag law- Spherical
	Physical models	Stochastic collision
		Coalescence
		TAB Break up
Materials	Fluid	Air
	Solid	Aluminum
	Inert particle	Water-liquid

Table C.1: Model settings

Boundary conditions	Velocity-inlet	Velocity magnitude- 10m/s Turbulent intensity- 10% DPM- escape
	Pressure-outlet	Turbulent intensity- 10% DPM- escape
	Outer wall	Stationary wall DPM- reflect
	Cell walls	Stationary wall Moving wall- 200,2000,10000 rpm Rotational direction x=0, y=1, z=0 DPM- reflect
Operating conditions	Pressure Specified density Temperature	101325 Pa 1.225 kg/m3 288 K

Table C.2: Boundary conditions, operating conditions

Solution Methods	Pressure-velocity coupling Pressure discretization Momentum Turbulent kinetic energy Transient formulation	PISO PRESTO! First order upwind First order upwind First order implicit
Solution Controls	Pressure Density Body forces Momentum Turbulent kinetic energy Specific dissipation rate Turbulent viscosity Discrete phase sources	0.3 1 1 0.7 0.8 0.8 1 0.5

Table C.3: